Journal Pre-proof

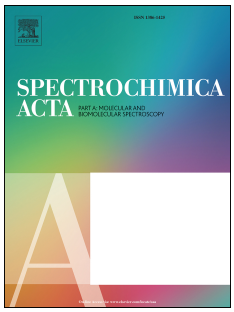

A novel Cu(II) distorted cubane complex containing Cu_4O_4 core as the first tetranuclear catalyst for temperature dependent oxidation of 3,5-di-*tert*-butyl catechol and in interaction with DNA & protein (BSA)

Zahra Asadi, Leila Zarei, Maryam Golchin, Eliska Skorepova, Vaclav Eigner, Zahra Amirghofran

PII: S1386-1425(19)30983-7

DOI: https://doi.org/10.1016/j.saa.2019.117593

Reference: SAA 117593

To appear in: *Spectrochimica Acta Part A: Molecular and Biomolecular Spectroscopy*

Received Date: 8 August 2019

Revised Date: 1 October 2019

Accepted Date: 1 October 2019

Please cite this article as: Z. Asadi, L. Zarei, M. Golchin, E. Skorepova, V. Eigner, Z. Amirghofran, A novel Cu(II) distorted cubane complex containing Cu_4O_4 core as the first tetranuclear catalyst for temperature dependent oxidation of 3,5-di-*tert*-butyl catechol and in interaction with DNA & protein (BSA), *Spectrochimica Acta Part A: Molecular and Biomolecular Spectroscopy* (2019), doi: https://doi.org/10.1016/j.saa.2019.117593.

For Table of Contents Only

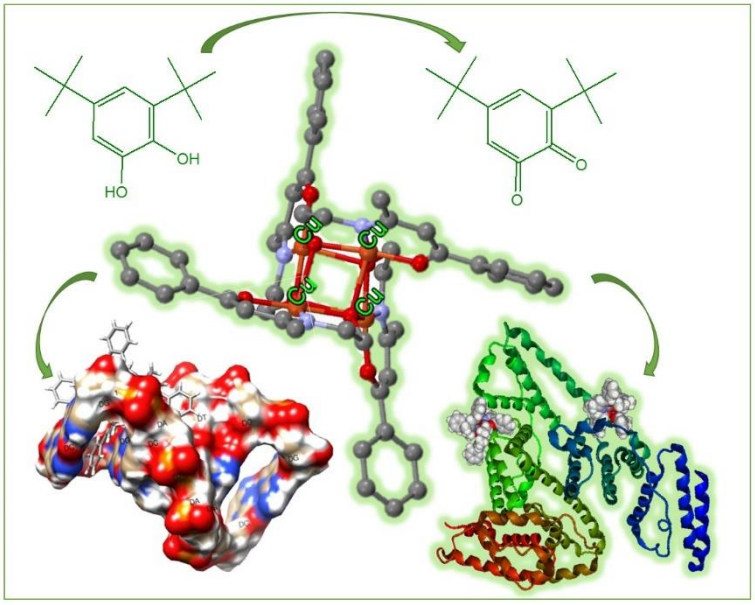

A new synthesized tetra-nuclear Cu(II) distorted cubane complex containing Cu_4O_4 core; nominated ($[CuL]_4$); exhibited excellent catecholase activity in aerobic oxidation of 3,5-di-*tert*-buthyl catechol to its o-quinone. The kinetics and mechanism of the oxidation of 3,5-$DTBCH_2$ catalyzed by the complex, were studied at four different temperatures. Interaction of complex with FS-DNA and bovine serum albumin (BSA) was investigated. *In vitro* anticancer activity of the complex and DNA cleavage activity was evaluated.

A novel Cu(II) distorted cubane complex containing Cu_4O_4 core as the first tetranuclear catalyst for temperature dependent oxidation of 3,5-di-*tert*-butyl catechol and in interaction with DNA & protein (BSA)

Zahra Asadi[*a], *Leila Zarei*[a], *Maryam Golchin*[a], *Eliska Skorepova*[b], *Vaclav Eigner*[b], *Zahra Amirghofran*[c]

a) Department of Chemistry, College of Sciences, Shiraz University, Shiraz 71454, Iran

b) Institute of Physics ASCR, v.v.i, Na Slovance 2, 182 21 Prague, Czech Republic

c) Department of Immunology and Autoimmune Diseases Research Center, Shiraz University of Medical Sciences, Shiraz 71454, Iran

Abstract

The tri-dentate Schiff base ligand 3-(2-hydroxyethylimino)-1-phenylbut-1-en-1-ol (L) produced the tetra-nuclear Cu(II) distorted cubane complex which contain Cu_4O_4 core, upon reaction with Cu(II)acetate.H_2O. The complex was structurally characterized by X-ray crystallography and found that, in this tetrameric and tetra-nuclear distorted cubane structure, each two-fold deprotonated Schiff base ligand coordinated to a Cu(II) center with their alcoholic oxygens and imine nitrogens and formed six and five-membered chelate rings. At the same time,

* Corresponding author. E-mail address: zasadi@shirazu.ac.ir

Tel: +98 713 6137118; Fax: +98 713 646 0788

each ligand bridged to a neighboring Cu(II) atom by its alcoholic oxygen, thus the metal centers became penta-coordinated. The copper(II) complex with μ-η^2-hydroxo bridges and Cu….Cu distance about 3Å was structurally similar to the active site of natural catechol oxidase enzyme and exhibited excellent catecholase activity in aerobic oxidation of 3,5-di-*tert*-butyl catechol to its o-quinone. The kinetics and mechanism of the oxidation of 3, 5-DTBCH_2 catalyzed by $[CuL]_4$ complex, were studied at four different temperatures from 283 to 313K by UV-Vis spectroscopy. Interaction of $[CuL]_4$ complex with FS-DNA was investigated by UV-Vis and fluorescence spectroscopy, viscosity measurements, cyclic voltammetry (CV), circular dichroism (CD) and agarose gel electrophoresis. The main mode of binding of the complexes with DNA was intercalation. The interaction between $[CuL]_4$ complex and bovine serum albumin (BSA) was studied by UV-Vis, fluorescence and synchronous fluorescence spectroscopic techniques. The results indicated a high binding affinity of the complex to BSA. *In vitro* anticancer activity of the complex was evaluated against A549, Jurkat and Ragi cell lines by MTT assay. The complex was remarkably active against the cell lines and can be a good candidate for an anticancer drug. Theoretical docking studies were performed to further investigate the DNA and BSA binding interactions.

Keywords: Cu(II) cubane complex; catecholase activity; FS-DNA; BSA; docking study; anticancer activity.

Introduction

Currently, metal-organic molecules are developed by using organic/inorganic bridging ligands, which create di- or poly-nuclear clusters, by one-, two- or three-dimensional self-assembly [1, 2]. The organic ligands and the reaction conditions effect on the composition and

topology of the molecules. Among the poly-nuclear clusters, tetranuclear copper (II) complexes with a Cu_4O_4 cubane core are particularly interesting. These complexes have medium size; they are not as small as simple binuclear complexes, nor as large as the bulky poly-nuclear complexes, which effects the magnetic properties of these complexes. Cubane-like complexes are classified according to two different methods based on the Cu-O distances [3] and the Cu….Cu distances [4].

Cu complexes have been used in various areas of research, such as crystal engineering [5, 6] supramolecular chemistry, molecular magnetism [7, 8], to mimic the active sites of metallo-enzymes and as an anti-cancer treatment [9-13]. Since the discovery of *cis-platin* as an efficient anticancer drug, the pharmaceutical research has focused on other metal-based drugs for cancer therapy [14, 15]. Because of the serious side effects of *cis-platin* as a covalent DNA binder [16], researchers now focus on the less toxic, more-efficient and target-specific anticancer drugs with non-covalent mode of binding. The most important limitations of the drugs under development are their side-effects and cell membrane resistance [17]. Copper (II) complexes are promising anticancer drugs of this type. Up to now, DNA-binding, cytotoxicity, the ability of DNA-cleavage and the possible utility of the Cu(II) complexes in photodynamic therapy have received considerable attention.[18-23] Recently many researches focused on the interaction of copper(II) complexes with serum albumins, e.g. BSA & HSA, because, same as for DNA, proteins are one of the targets for anticancer drugs [9, 18, 24-26].

Beside the potential for the cancer treatment, we have decided to study also the catecholase oxidation activity of our Cu complex. The oxidation of reagents with the atmospheric oxygen in mild conditions is of great importance especially in synthetic and industrial processes. In biological systems, this is done by oxidation catalysts such as metallo-proteins, which contain

copper or iron metals [27]. In type (III) copper proteins, e.g. hemocyanin, tyrosinase, catechol oxidase, a coupled binuclear copper center is the active site. Certain copper(II) complexes with oxide bridges can oxidize different kinds of o-diphenols (catechols) to o-quinones with simultaneous $2e^-$ reduction of O_2 to H_2O [28]. This process is called the *catecholase activity*. The active site of the catecholase protein contains two copper (II) centers (Cu….Cu distance is about 2.9Å), which are connected through di-μ-hydroxo bridges. Each Cu(II) center has a trigonal pyramidal structure with three histidine nitrogens. To mimic the catecholase activity of the bicopper(II) complexes, the structural parameters must be considered. The geometry of bicopper(II) complexes affects the catalytic activity [29]. For example, the mononuclear square-planar copper(II) complexes are less active than mononuclear non-planar copper(II) complexes. In the binuclear copper(II) complexes, the Cu….Cu distance must be less than 5Å for the activity to be retained. One explanation is that, for the electron transfer to be possible, the two metal centers must be in an appropriate distance, in which it is possible for the two hydroxyl oxygen atoms of catechol to bind to the metals and act as a bridging ligand [10].

We have chosen 3,5-di-*tert*-butylcatechol as a suitable model substrate to identify new efficient oxidation catalysts. Considering the above-explained geometric requirements, we aimed to synthesize model complexes containing at least two copper centers in close proximity.

Overally, according to the importance of synthesizing the artificial enzymes, and because of the significance of mimicking the anti-cancer metal-based drugs, designing a complex with all these properties is a success. Thus, in this paper we synthesized and characterized a tetra-nuclear copper(II) complex with μ-η^2-hydroxo bridge as a potential structural and functional model for the active site of the catechol oxidase enzyme. We also provide the results related to the

copper(II) complexes ability to function as anti-cancer agents, particularly the affinity of the complex to bind to HS-DNA & BSA and the ability of the complex for DNA cleavage.

Experimental Section

Material and methods

All used materials, instruments and reaction conditions are mentioned in the supporting information.

Synthesis and characterization

The Synthesis route of 3-(2-hydroxyethylimino)-1-phenylbut-1-en-1-ol (L) (Fig. S1) and $[CuL]_4$ complex with ^{1}HNMR, FT-IR, Elemental Analysis, UV–Vis. spectral data of the compounds are mentioned in the supporting information.

X-ray structure analysis

A saturated solution of the complex in a mixture of chloroform and n-hexan solvents was allowed to evaporate at room temperature for two weeks and then green crystals of tetranuclear copper compound were obtained. The X-ray diffraction measurements were carried out at 120K on a Xcalibur, Gemini ultra diffractometer using the MoKα radiation ($\lambda = 0.71073$ Å) from a fine-focus sealed X-ray tube with a graphite monochromator and CCD detector Atlas S2. The data were corrected for absorption using the CrysAlisPro software. The structure was solved by the charge-flipping method by program Superflip [30] and refined by full matrix least squares on F^2 with JANA2006 program [31].

Catecholase activity

The catalytic activity of $[CuL]_4$ complex for oxidation of 3,5-di-tert-butylcatechol (3,5-DTBCH2) to 3,5-ditert-butylquinone (3,5-DTBQ) under aerobic condition (using only atmospheric oxygen) were monitored spectrophotometrically by using a Lambda 25 Perkin–Elmer spectrophotometers. The reaction conditions and formulas are mentioned in the supporting information.

DNA binding studies, Molecular docking of DNA, DNA cleavage experiment and ethidium bromide (EB) competitive study, Protein-binding studies, Molecular docking to proteins

The reaction conditions and methods of the experimental and theoretical studies are mentioned in the supporting information.

***In vitro* anticancer studies**

The cytotoxic effects of the complex against various cell lines comparing with cis-platin were examined using 3-(4,5-dimethylthiazol-2-yl)-2,5-diphenyltetrazoliumbromide (MTT) colorimetric assay as previously described [32]. Cell lines including Jurkat (human T cell leukemia), Raji (Burkitt's lymphoma) and A549 (lung carcinoma) were cultured in RPMI 1640 medium (Sigma, St. Louis, MO) containing 10% fetal calf serum (Gibco, Berlin, Germany) at 37ºC in a CO_2 incubator until confluent. Jurkat and Ragi cells at 15×10^3 cells/100µl and A549 cells at 7.5×10^3 cells/100µl were seeded into 96-well culture plates in triplicate. Cells were treated with various concentrations of the complex (0.1–100 µg/mL) for 48 h. Negative control was cells treated only with DMSO solvent at a concentration equal to the test wells and positive control was cells treated only with cis-platin. After incubation time, 10µL MTT solution (5mg mL^{-1} in RPMI medium) was added for 4 h and then cells treated with 100 µl DMSO to dissolve formazan crystals while shaking. The optical density (OD) of the wells were measured at 570nm

with a 630nm reference wavelength using a microplate reader (Bio-Tek's, VT). The percent inhibition of cell growth was calculated using the following formula; [1– (test OD/negative control OD)] × 100. Fifty percent cell growth inhibition (IC_{50}) values were determined from percent inhibition graph for different concentration the complex.

Results and discussion

Synthesis and characterization of compounds

Synthesis route of $[CuL]_4$ complex is shown in Scheme 1. Schiff base ligand (L) was synthesized by the condensation of benzoylacetone and 2-aminoethanol in 1:1 mole ratio. L seems to behave as a tridentate ligand. After addition of Cu(II) acetate to the ethanolic solution of L, a cubane like complex was synthesized. The affinity of Cu(II) center for a penta-coordinated geometry with John-teller distortion produced a distorted cubane complex containing Cu_4O_4 core.

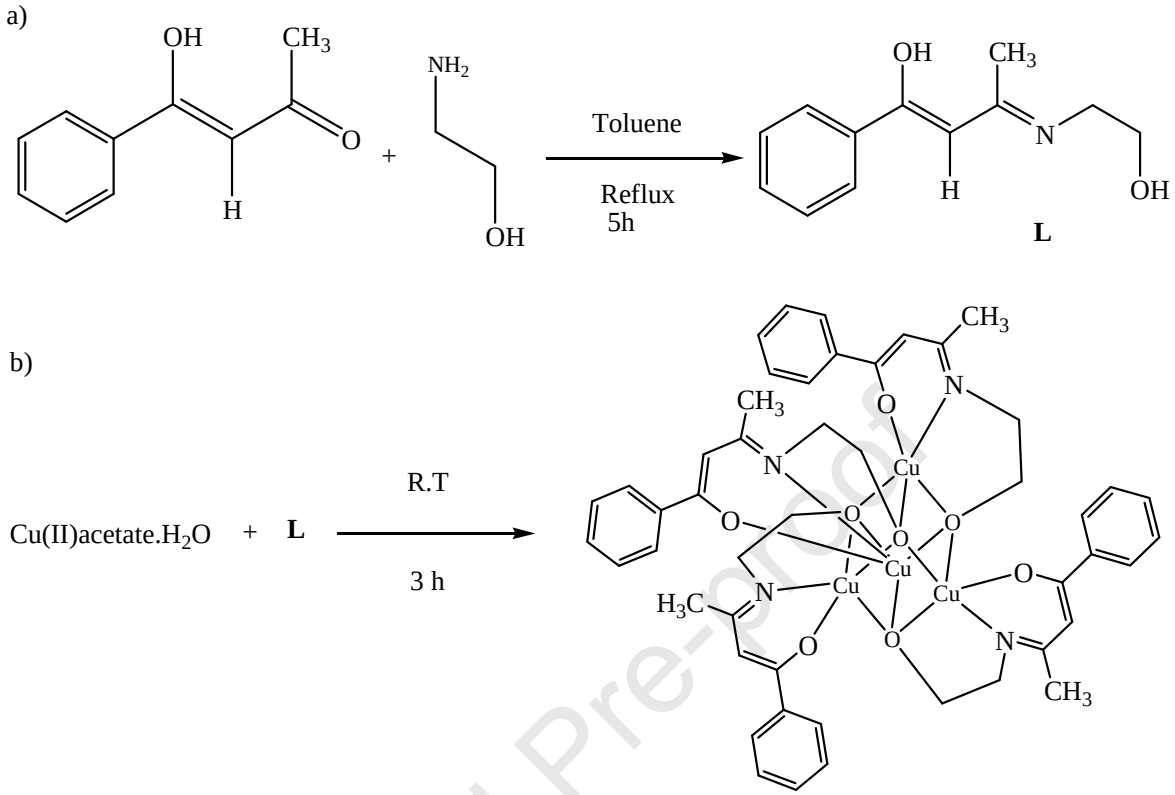

Scheme 1. Synthesis route of $[CuL]_4$ complex.

The synthesized ligand and complex were identified by FT-IR, ^{1}H NMR and elemental analysis. Redox properties of the Cu(II) complex were studied by cyclic voltammetry. The single-crystals of complex were prepared for X-ray crystallography. The complex was stable in atmosphere and soluble in DMSO, methanol and ethanol and insoluble in non-polar solvents.

^{1}H NMR spectrum of 3-(2-hydroxyethylimino)-1-phenylbut-1-en-1-ol (L) carried out in DMSO-d_6 (Fig. S2) and $CDCl_3$ (Fig. S3). In DMSO-d_6, a singlet signal for OH^a at 11.34 ppm and a multiple signal for aromatic protons at 7.81-7.40 ppm were observed additionally, a singlet signal at 5.72 ppm for C=CH, a multiple signal at 4.93 ppm for OH^b and a triplet signal for CH_2^a protons at 3.55 ppm (CH_2^b was hidden under DMSO signal) and a singlet signal for the methyl protons at 2.05 ppm were assigned. In order to distinct between the signals of OH^b and H^a one

drop of D_2O was added to the DMSO-d_6 solution of L. Hydrogen bonding between OH^a, OH^b and D_2O removed the related signals of hydroxyl groups. On the other hand, hydrogen bonding caused a slight shift for DMSO signals and so the signal of CH_2^b could be seen at 3.52 ppm and CH_2^a at 3.35 ppm in this spectrum (Fig. S2). To confirm the existence and the signal positions of CH_2^a and CH_2^b, ^1H NMR analysis in $CDCl_3$ was repeated. In this spectrum, a singlet signal for OH^a at 11.51 ppm, a multiple signal for aromatic protons at 7.85-7.37 ppm, a singlet signal for C=CH proton at 5.66 ppm, a triplet signal for CH_2^a protons at 3.83 ppm, a quartet signal for CH_2^b at 3.48 ppm, a singlet signal for OH^b at 2.62 ppm and a singlet signal for the methyl protons at 2.05 ppm were observed (Fig. S3).

FT-IR spectrum of the 3-(2-hydroxyethylimino)-1-phenylbut-1-en-1-ol (L) (Fig. S4) was indicated by the presence of strong imine (C=N) bands at 1604 cm^{-1} and OH vibrations at 3328 cm^{-1} [33, 34]. In the complex (Fig. S5), $\upsilon_{C=N}$ was generally shifted to lower frequencies relative to the free ligand, indicating a decrease in the C=N bond order due to the coordination of the imine nitrogen to the metal and back bonding from the Cu(II) to the π^* orbital of azomethine group [35]. Also, C-O stretching vibrations shift toward lower values as a result of coordination of the oxygen to the metal ion [34]. Vibrations around 3448 cm^{-1} was attributed to the presence of lattice and coordinated water [36]. Medium-weak bands at 3062 cm^{-1} is related to (C-H) modes of vibrations [37]. The ring skeletal vibrations (C=C) were consistent in the region of 1440–1465 [38]. In the lower frequency region medium-weak bands observed at 551–563 and 435–458 cm^{-1} which have been assigned to (M–N) and (M–O) vibrations, respectively [39, 40].

The UV-Vis spectra (200-700nm) of the ligand in Tris-HCl buffer solution (pH 7.2) (10 μM) and complex in methanol/Tris-HCl buffer solution (30 μM) were recorded. The electronic absorption spectrum of the complex, displayed three specific absorption bands. Two absorption

bands at 209 and 256 nm were assigned to the π-π* transition in aromatic rings and azomethine groups. The first band at higher energies were attributed to π→π* transitions associated with the phenyl ring and the second band at lower energy arise from π→π* transitions associated with the carbonyl and azomethine chromophores. A wide intense absorption band at 346 nm was attributed to the n-π* transition in carbonyl group and oxygen of Schiff base to phenyl ring (Fig. S6). For the free ligand, the band in the region 346 nm was attributed to the n→π* transition of the imine chromophore, and the band in the higher energy region at 247 nm was assigned to the π→π* transition of the phenyl ring [41-44] (Fig. S7).

Crystal structure of $[CuL]_4$

The molecular structure of tetra-nuclear copper (II) complex along with atom labeling is shown in Fig. 1. Crystallographic data and bond lengths and bond angles of the complex are listed in Tables 1 and S1.

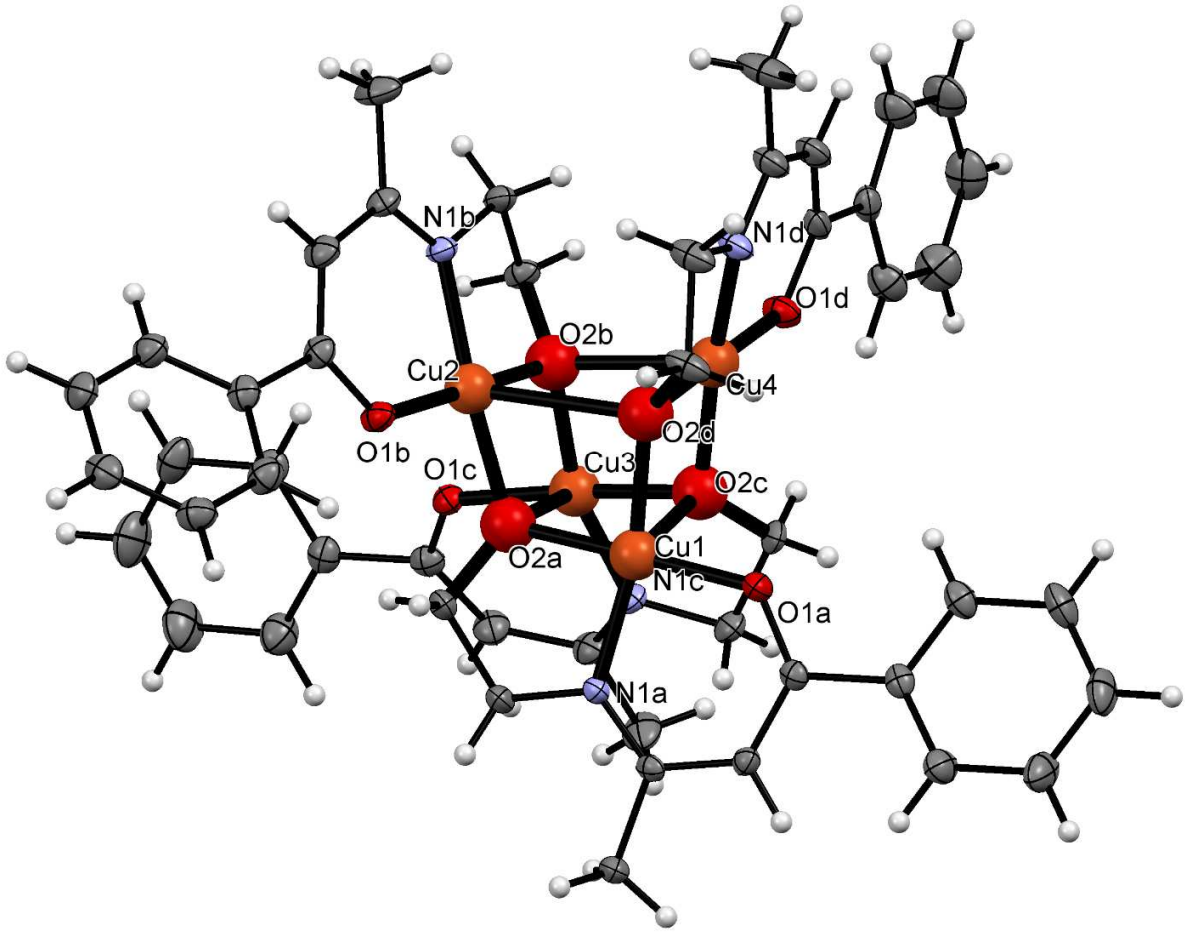

Fig. 1. The $[CuL]_4$ complex with thermal ellipsoids at 50% probability level (except the cubane cube, which is highlighted and displayed as balls) and the atom-labeling scheme. The labels of H and C atoms are omitted for clarity.

Table 1. Crystal data and structure refinement for $[CuL]_4$ complex

Formula of refinement model	C48 H52 Cu4 N4 O8, 3.195(O)
Temperature [K]	120
Crystal system	Trigonal
Space group	R 3

a [Å]	29.951(1)
b [Å]	29.951(1)
c [Å]	14.7438(5)
α [˚]	90
β [˚]	90
γ [˚]	120
V[Å^3]	11454.1(7)
Z	9
D[gcm^{-3}]	1.459
μ [mm^{-1}]	1.709
F(000)	5162.0
R(F^2>3σ) (reflections)	0.0203 (12347)
wR(F^2) (reflections)	0.0579 (12936)

The synthesized complex created a tetrameric and tetra-nuclear cubane complex, in which each two-fold deprotonated Schiff base ligand coordinated to a Cu(II) center with their hydroxyl oxygen and imine nitrogen atoms and formed six and five-membered chelate rings. At the same time, each ligand bridged to a neighboring Cu(II) atom by its hydroxyl oxygen (CH_2CH_2OH) thus the metal centers were penta-coordinated (three donor atoms from one Schiff base ligand,

two oxygens from two other neighboring Schiff base ligands). The torsion angles between six and five-membered chelate rings were in the range ±178.7-179.8° confirming that these two rings were almost coplanar (Fig.2) (Table S1).

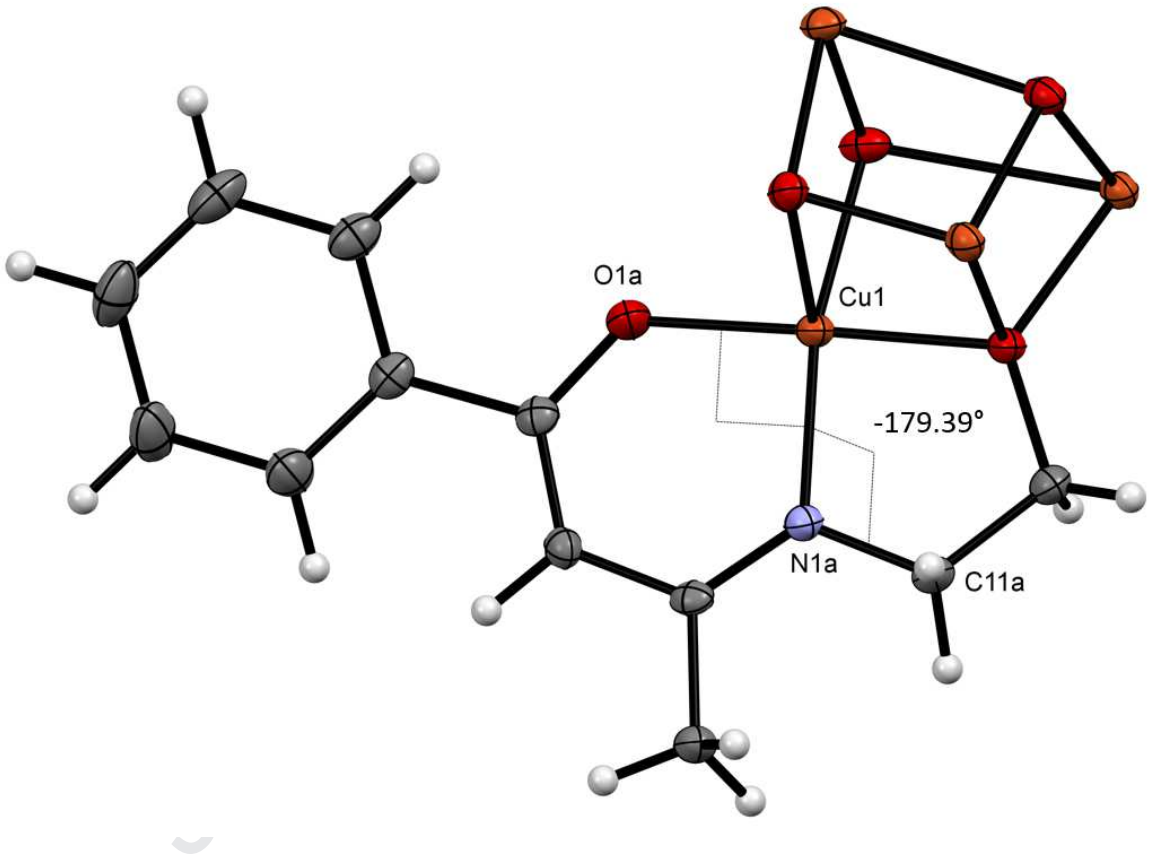

Fig. 2. The torsion angle between six and five-membered chelate rings.

The tetramer formed as a distorted cube, in which four Cu(II) atoms and four oxygen atoms alternatively occupied the vertices. In this distorted cube, four of the twelve edges (Cu-O bonds) were longer. The eight Cu-O shorter bonds were about 1.9 Å and out of the longer ones, three were about 2.3 Å and one was 2.592 Å. Because the six Cu….Cu distances are all similar and about 3 Å in the distorted cube (Cu1….Cu2 = 3.246 Å, Cu1….Cu3 = 3.253 Å, Cu1….Cu4 =

3.097 Å, Cu2….Cu3 = 3.130 Å, Cu2….Cu4 = 3.388 Å, Cu3….Cu4 = 3.138 Å) the structure is classified as [6+0] cubane complex [4] (Fig. S8).

The geometry around each Cu(II) center was a distorted square pyramid (Fig. S9) with τ values of 0.17, 0.06, 0.19, 0.16 for Cu1, Cu2, Cu3, Cu4, respectively. A. W. Adison et.al [45] determined τ=1 for a regular trigonal bipyramide and τ=0 for a regular square pyramide by using the formula: $\tau = \frac{(\beta-\alpha)}{60}$ where α, β are the angles between each trans donor atoms forming the plane in a square pyramidal geometry (Table 1). τ value is applicable for five coordinate structures.[45] By comparing the τ values, we see that distortion from square pyramidal structure around Cu2 was less than around the other Cu centers. Moreover, the degree of distortion from square pyramidal structure for Cu1, Cu3, Cu4 was almost the same. The four basal positions of each square pyramide around a Cu center contained three oxygen and a single nitrogen atom. An oxygen occupied the apical position. Bond length of basal Cu-O and Cu-N were 1.906-1.967 Å. The bond lengths for the apical Cu-O were in the range 2.375-2.592 Å due to Jahn-Teller distortion.

The packing diagram of complex is shown in Fig. 3. Nine independent distorted cubane are packed in a unit cell (Z=9). There are no regular H-bond donors present in the complex, so there is no H-bonding present in the structure. Neighboring $[CuL]_4$ units are connected through edge-to-face π-π interactions between the benzene rings of the ligand. Beside the complex itself, the structure contains disordered low-occupancy water molecules as a solvent, making the structure a non-stoichiometric hydrate. On average, there are 3.195 water molecules per one $[CuL]_4$ complex.

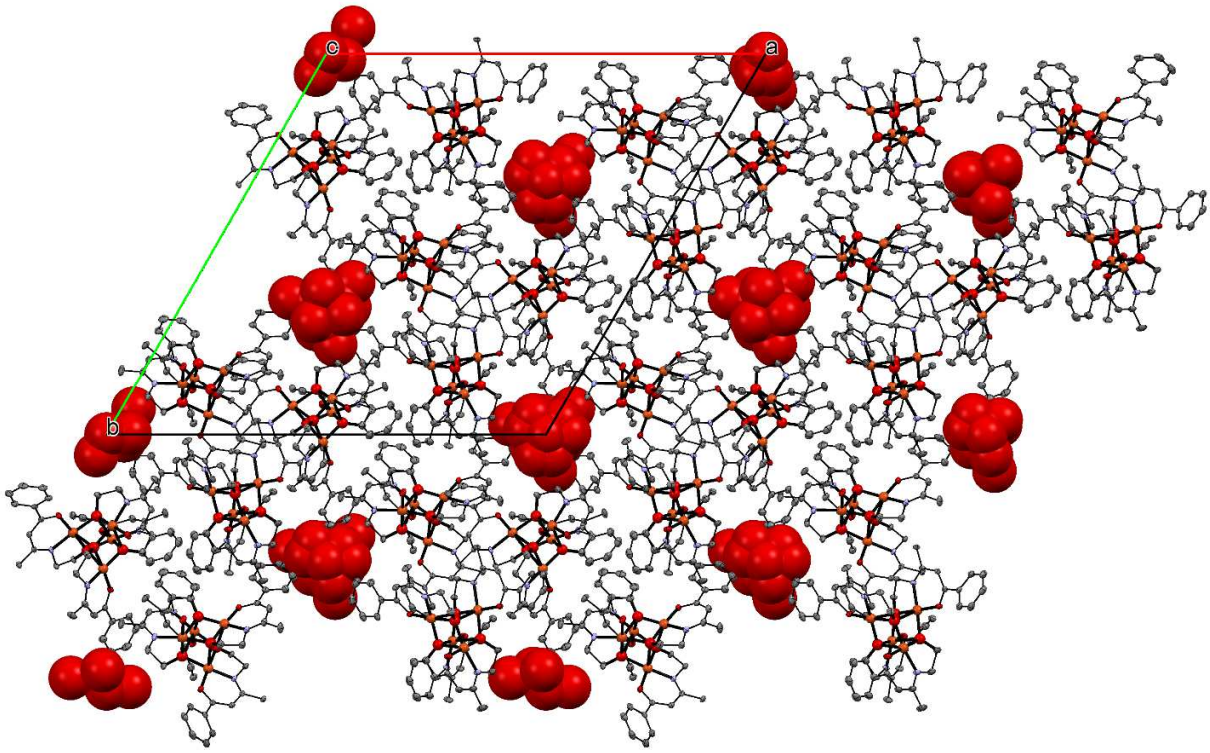

Fig. 3. Crystal packing of the complex. Disordered water molecules shown as red balls.

Kinetic studies of catecholase activity

Mechanistic studies on catechol oxidation by the $[CuL]_4$ complex. The substrate 3,5-di-*tert*-butylcatechole was used to study the catecholase activity of the model complex $[CuL_4]$ because of its low redox potential which accelerate its oxidation to the corresponding quinone and the presence of bulky *tert*-butyl substituents which prevent further reactions such as ring-opening and polymerization and also the stability and presence of a characteristic band around 400nm of the resulted quinone that help the monitoring of the reaction. (Scheme S1)

Different approaches have been proposed for the mechanism of catecholase activity of Cu(II) complexes base on the crystallographic, spectroscopic, structural and chemical evidence. For the initial step, deprotonated catechol or its derivatives should bind to Cu(II) center(s). Different

binding modes of the catechol (or deprotonated catechol) to copper(II) centers has been proposed as: i) η^2 chelating catechol, ii) η^2:η^1 bidentate bridging, iii) *syn-syn* bidentate bridging, iv) *anti-anti* bidentate bridging, etc [10]. According to structural properties (metal-metal distances, nature of bridging ligands between Cu centers, rigidity of the structure) and electrochemical properties of the complexes, each mode of binding mentioned above is possible. However, it was reported that the highest catecholase activity was observed for the complexes, which bound catechol in a bidentate bridging manner. It means that the Cu…Cu separation in these complexes must be less than 4 Å, otherwise simultaneous binding of catechol to both Cu centers is prevented. It is worth noting that small bridging ligands bring Cu centers to the close proximity of each other and thus promote the catalytic activity. Examples of such bridging ligands are: hydroxides, alkoxides, and phenoxides [10].

In the $[CuL]_4$ complex, hydroxide moiety of the Schiff base ligands bridge between three Cu(II) centers and bring them close to each other. All the Cu...Cu distances are in the range 3.097-3.388 Å, which allow 3, 5-ditertbutylcatecholate dianion to bind as a bridging ligand in a *syn-syn* fashion (Fig. S10).

Casella and co-workers [46] proposed two consecutive steps for the catalytic reaction including step one: a fast stoichiometric reaction between a molecule of 3,5-$DTBCH_2$ and dicopper(II) complex and step two: a slower catalytic reaction. They also proposed that, in the first stoichiometric step, electron transfer between the bound catechol and dicopper(II) centers occurred, thus, the first step, to some extent, is dependent to Cu^{II}/Cu^{I} redox potential. In the catalytic process, two copper (II) centers reduce to copper (I) simultaneously and one molecule of 3, 5-$DTBCH_2$ is then oxidized to the related quinone molecule. Dicopper (I) centers reoxidize

to copper (II) centers in a relatively slow step in the presence of O_2. A proposed cycle of mechanism is shown in Scheme 2.

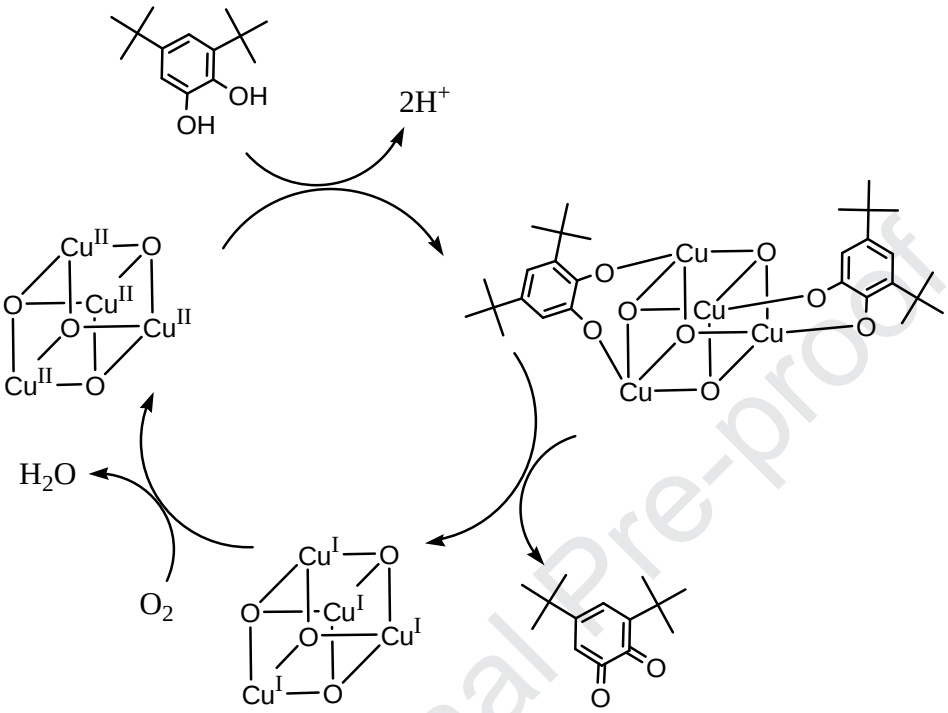

Scheme 2. Catalytic cycle for the oxidation of 3, 5-DTBCH_2 catalyzed by $[CuL]_4$ complex.

To confirm this hypothesis, we have performed the following: In a typical procedure; after mixing 3, 5-DTBCH_2 with the complex, the spectral changes at intervals of 4 min were monitored (Fig. 4). The quinone band at 410 nm grew; therefore, the oxidation of catechol has occurred.

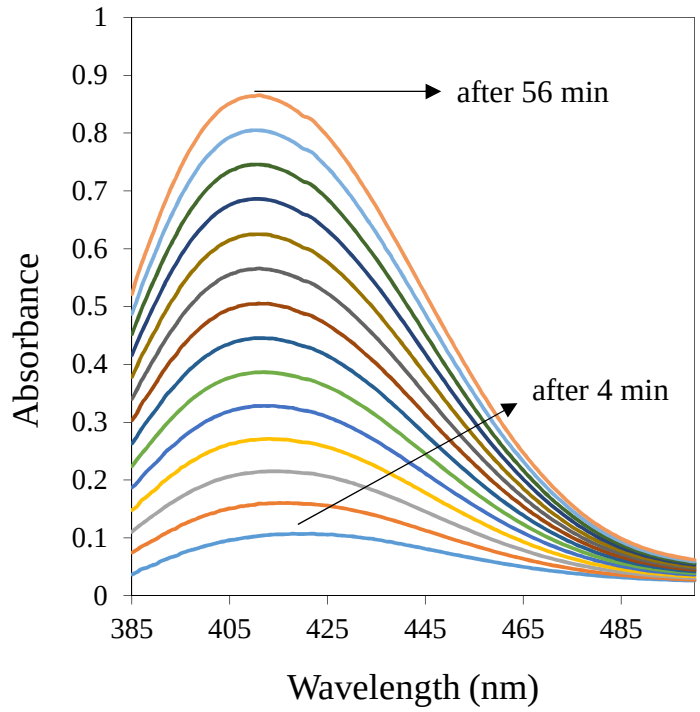

Fig.4. Spectral profile showing the increase of quinone band at about 410 nm after the addition of 600 fold of 3,5-DTBCH$_2$ to a solution of complex (50µM) in DMF at 283K. Spectra were recorded after each 4 min.

The kinetics of the oxidation of 3,5-DTBCH$_2$ catalyzed by [CuL]$_4$ complex were studied under pseudo first order conditions. The ratio of [3, 5-DTBCH$_2$]/[complex] varied from 10 to 800 fold, in which 3,5-DTBCH$_2$ concentrations were varied in the range 500 (µM) to 40000 (µM) and the complex concentration was constant at 50 µM. A first-order dependence was observed at these concentrations of the substrate. The experiments were done at four different temperatures from 283-313K, under aerobic conditions. The reaction process of the mixture of 3, 5-DTBCH$_2$ and complex at the maximum of the 3, 5-DTBQ band (410 nm) were followed for a period of 90 min. For the blank experiment containing 3,5-DTBCH$_2$ without catalyst, no formation of the 3,5-DTBQ was observed up to 2h in DMF. Pseudo-first-order rate constants

(k_{obs}) in different temperatures are available in Table 2. k_{obs} values during the temperature change from 283 to 303K were obtained in catechol concentrations from 0.01 to 0.04M (100-800 folds) and at 313K from 0.0005 to 0.008M (10-140 folds). At 313K, the reaction at catechol concentrations from 0.01 to 0.04M was too fast to obtain proper spectral changes thus lower concentrations of catechol were used. These clearly revealed that the catecholase activity of the complex $[CuL]_4$ is temperature dependent.

Table 2. Pseudo-first-order rate constants, $10^4 k_{obs}$[a](s^{-1}), for the oxidation of 3,5-DTBCH_2 (0.0005-0.04 M) catalyzed by $[CuL]_4$ complex (50µM) in DMF at different temperatures (283-313K).

[catechol] (M) / T(K)	0.0005	0.002	0.0035	0.005	0.0065	0.008	0.01	0.015	0.02	0.025	0.03	0.035	0.04
283								0.55 (0.01)	0.63 (0.01)	0.68 (0.01)	0.72 (0.01)	0.78 (0.01)	0.82 (0.01)
293							0.69 (0.02)	0.87 (0.02)	0.95 (0.02)	1.14 (0.01)	1.22 (0.02)	1.33 (0.01)	
303				0.97 (0.01)			1.01 (0.01)	1.24 (0.01)	1.55 (0.01)	1.70 (0.04)	1.95 (0.07)		
313	1.13 (0.01)	1.23 (0.02)	1.33 (0.01)	1.46 (0.02)	1.54 (0.03)	1.65 (0.09)							

a) The numbers in parentheses are the standard deviations of k_{obs}.

k_2 values are obtained from the slope of the linear plots of k_{obs} *versus* [catechol] (Fig. S11). By increasing the temperature, k_2 values increased ($10^3 k_2$ = 1.06 (283K), 2.55 (293K), 4.17 (303K), 6.95 (313K)) indicating an endothermic oxidation reaction which might be very important in designing more efficient catecholase model complexes.

The activation parameters were obtained from Eyring plots of $\ln(k_2/T)$ *vs.* 1/T at four different temperatures (Fig. S12). The positive value of free energy at 293 K ($\Delta G^{\#} = \Delta H^{\#} - T\Delta S^{\#}$ =28.705 KJ mol^{-1}) indicated that the oxidation process was nonspontaneous. The positive $\Delta H^{\#}$ values (42.788 KJ mol^{-1}) confirmed endothermic process and the positive value of $\Delta S^{\#}$ (48.064 J mol^{-1} K^{-1}) revealed that the disorder of the system was raised during the process due to the

production of H_2O molecules. In each catalytic cycle, one mole of 3, 5-DTBCH_2 produced one mole of 3, 5-DTBQ, successively, atmospheric O_2 diffuse in the solution and one mole of H_2O was produced, thus the disorder of the medium was increased.

To investigate the enzymatic kinetics of catecholase activity of various copper(II) complexes Michaelis–Menten equation was used repeatedly. Many reports in this field revealed that the reaction rate might be dependent to the concentration of the substrate (catechol), the kind of catalyst (metal complex), the concentration of dioxygen in the reaction medium and the kind and concentration of some additives such as dyhydrogenperoxide and Kojic acid[10]. It is worthy to mention that few studies repot the dependence of the reaction rate to the catalyst concentration [47].

Similar to other enzymatic mimicking complexes, $[CuL]_4$ revealed saturation kinetics and the treatment was investigated bases on Michaelis–Menten model. Michaelis−Menten constant (K_M), maximum initial rate (V_{max}) were calculated by Michaelis–Menten equation and Lineweaver–Burk plot [48] (Fig. S13) . The turnover number (k_{cat}) value can be calculated by dividing the V_{max} value by the concentration of the complex. The determined kinetic data, $V_{max} = 4.7461\times10^{-5}$ $Mmin^{-1}$, $K_M = 0.0178$ M, and $k_{cat} = 56.95\ h^{-1}$.

Because the solvent is one of the main factors in the enzymatic activity of the catalysts, some kcat of various copper (II) complexes in DMF was reported for comparison: $[\{Cu_2L(\mu\text{-}OH)(H_2O)\}(\mu\text{-}ClO_4)]_n(ClO_4)_n$, $k_{cat} = 39.0h^{-1}$ [1]; $[\{Cu_2L(\mu_{1,1}\text{-}N_3)(ClO_4)\}_2(\mu_{1,3}\text{-}N_3)_2]$, $k_{cat} = 39.9h^{-1}$ [1] thus, $[CuL]_4$ complex is located in the upper range of functional models for catecholase active complexes.

DNA-binding studies

DNA is the primary pharmacological targets for anticancer drugs thus studying the interaction of metal complexes with DNA is of great importance. Different techniques are used commonly to study the binding strength and binding modes. Some of these techniques are purely experimental and some of them are theoretical.

Electronic absorption spectroscopic studies. In many DNA interaction studies, UV-Vis absorption spectroscopy has been employed as a simple instrumental technique, which is used for either studying the DNA stability or drug-DNA interactions. In this method the changes in UV-Vis absorption spectra of the drug (complex) or DNA is monitored. An easy way to investigate the interaction between drug and DNA, is comparing the shift in the maximum of the absorption band of drug when it is free in solution or is bound to DNA [49]. The extent of this shifting could be related to the strength of the interaction between DNA and drug. Fig. 5 describes the interaction of our complex with DNA. The absorption band at 346nm revealed hypochromism. Also two isosbestic points near 367 nm and 302 nm were recognized. These spectral changes suggest covalent binding of complex to DNA or intercalation, in which a strong stacking interaction between the aromatic chromophore of the complex and base pairs of DNA has occurred [19]. The absorption band at 346 nm revealed a blue shift about of 6 nm along with hyperchromism (21%). These spectral changes correspon to groove binding of complex to DNA [50]. Hyperchromism along with hypsochromism suggest an electrostatic attraction or groove binding between Cu(II) complex and DNA which can cause changes in DNA conformation including partial uncoiling of the helix structure of DNA [51, 52].

Besides the qualitative investigation of the interaction, by calculating K_b, an insight into the quantitative behaviour was can be gained by using these equations (1a ,1b) [53, 54]

$$\frac{\varepsilon_a - \varepsilon_f}{\varepsilon_b - \varepsilon_f} = \frac{b - (b^2 - \frac{2K_b{}^2 C_t\,[DNA]}{s})^{1/2}}{2K_b C_t} \qquad (1a)$$

$$b = 1 + K_b C_t + \frac{K_b[DNA]}{2s} \qquad (1b)$$

In these equations, the absorption coefficients are denoted by ε_a, ε_b and ε_f for the absorption band (at a given DNA concentration) for the complex in its free form and for the complex in the fully bound form, respectively. K_b and s values were obtained by nonlinear least squares fitting of the experimental data to Eqs. (1a, 1b). The observed binding constant (10^4 M^{-1}) corresponds to the intercalation binding mode of interaction suggested above.

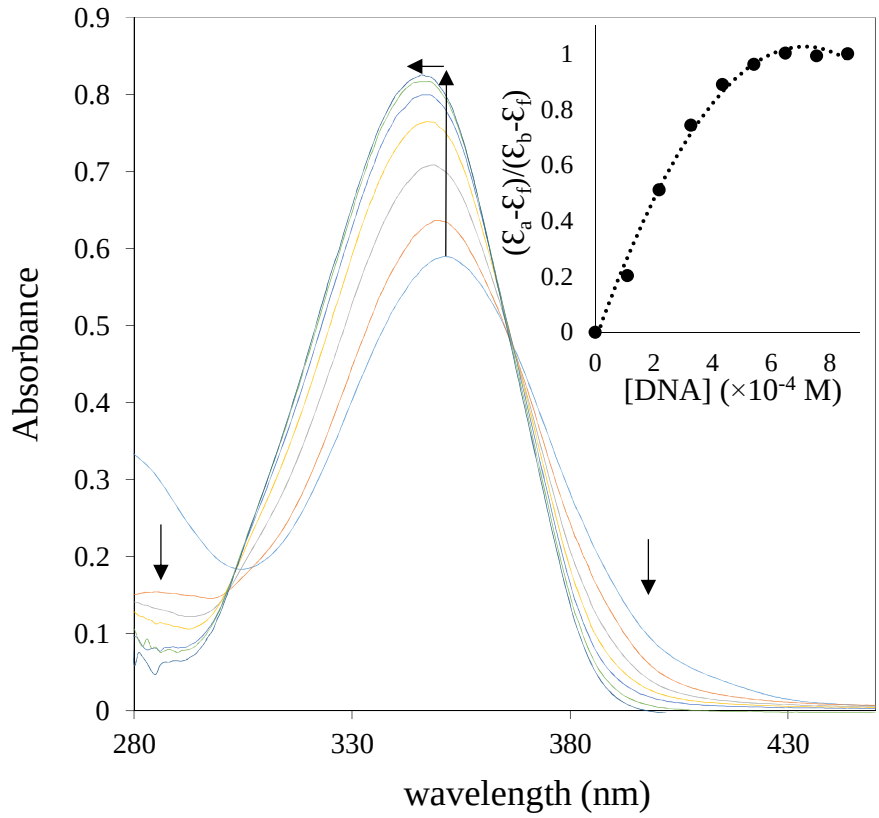

Fig. 5. Absorption spectra of the complex (12 μM) in DMSO, in the absence and presence of increasing amounts of DNA (0-110-220-330-430-540-650-750 and 860 μM). Inset: plot of ($Ɛ_a$-$Ɛ_f$)/($Ɛ_b$-$Ɛ_f$) vs.[DNA].

The intrinsic binding constant was calculated as $K_b=1\times10^4$ M^{-1} and *s* value is 1.5. The K_b value for ethidium bromide as a classical intercalator is 1×10^7 M^{-1}, which is much larger than the K_b of $[CuL]_4$ complex. It is worthy to note that the K_b value for $[CuL]_4$ complex is comparable to some transitional metal complexes either mono- or multi-centers, which were bound to DNA through intercalation or groove binding mode. For example: $[Cu_2(nap)_4(H_2O)_2]$ $K_b=2.27\times10^4M^{-1}$, $[Cu_2(dicl)_4(H_2O)_2]$ $K_b=1.74\times10^4M^{-1}$, $[Cu(nap)_2(bipy)]$ $K_b=3.86\times10^4M^{-1}$ $[Cu(dicl)_2(phen)]$ $K_b=1.81\times10^4M^{-1}$ with intercalation mode of binding and the K_b values of all compounds were lower than that of the classical intercalator [55]. [Cu (imda) (5,6-dmp)] $K_b=3.9\times10^3$ bound to

DNA through groove binding and [Cu (imda) (dpq)] $K_b=1.7\times10^4$ through partial intercalation [56]. [Cu (tdp) (bpy)]$^+$ $K_b=7.1\times10^3M^{-1}$, [Cu (tdp) (phen)]$^+$ $K_b=9.0\times10^4M^{-1}$, [Cu (tdp) (tmp)]$^+$ $K_b=7.0\times10^5M^{-1}$, [Cu (tdp) (dpq)]$^+$ $K_b=9.0\times10^5M^{-1}$ are examples of complexes with intercalation mode of binding.[18]

Viscosity measurements. A critical test in proposing the mode of binding of the small molecules to DNA is the viscosity measurement, which is a hydrodynamic measurement that is very sensitive to the DNA length change. Classical intercalators locate between DNA base pairs and cause an increase of the length of DNA and concomitantly its viscosity. However, non-classical intercalators cause bending (or kinking) of the DNA helix and reduce the length of DNA and concomitantly its viscosity. Groove binders, which bind in the grooves of DNA, cause less changes (positive or negative) or no changes in DNA viscosity [57, 58]. The values of relative specific viscosity $(\eta/\eta_0)^{1/3}$, where η is viscosity of pure DNA and η_0 is the viscosity of DNA in the presence of the different concentration of complex, were plotted against r (r = [complex]/[DNA]). From (Fig. S14), it is concluded that non classical intercalation (i.e. van der Waals interactions, groove binding or external binding) was the main mode of binding [59, 60].

Fluorescence studies (competitive binding affinity of the complex with ethidium bromide). A common fluorescence probe, which can bind to DNA, is ethidium bromide (EB), a planar cationic dye. In the presence of DNA, the fluorescence of EB increases according to its intercalation between adjacent DNA base pairs. If the enhanced fluorescence quenches by addition a second molecule, it competes with EB in binding to DNA. The base of displacement technique is the quenching of fluorescence due to the displacement of EB from the DNA sequence by another molecule. Quenching owns to the decreasing of the number of binding sites on the DNA, which had been occupied by EB. The extent of quenching of EB/DNA can be

correlated straightforward to the extent of binding of the second molecule to DNA *via* intercalation.[9, 19, 61, 62]

The fluorescence quenching spectra of the DNA-bound EB ([DNA]/[EB]=10) by addition of $[CuL]_4$ complex ([DNA]/[complex]=10, is shown in Fig. S15.

Quenching data were analyzed according to Stern−Volmer Equation 2 [63]:

$$\frac{I_0}{I} = 1 + K_q[Q] \qquad (2)$$

I_0 denotes the emission intensity in the absence of quencher and I the emission intensity in the presence of a quencher, K_q is the quenching constant, and [Q] is the quencher concentration. The K_q value is 1.77×10^5 that were obtained from the slope of the plot of I_0 /I versus [Q] (Inset Fig. S15). The value of apparent DNA binding constant (K_{app}) was calculated using Equation 3.

$$K_{EB}[EB] = K_{app}[Complex] \qquad (3)$$

where K_{EB} = 1.0 × 10^7 M^{-1} and [EB] = 1.25 μM [complex] is the concentration of complex causing a 50% reduction in the fluorescence intensity of EB. K_{app} calculated as 7.89×10^6 M^{-1}. The higher value of K_{app} revealed that $[CuL]_4$ bind to FS-DNA by intercalation.

Circular dichroism spectral analysis. It is obvious that during drug-DNA interactions the morphology of DNA changes to some extent. A useful technique for diagnosing these changes and proposing the mode of binding is circular dichroism (CD). It means that drug-DNA interactions can affect the structure of DNA and thus the intrinsic CD spectrum of DNA must be changed. The intrinsic CD spectrum of FS-DNA is characterized by a positive band at 275 nm assigned to the base stacking and a negative band at 245nm assign to the right handed helicity of B-form DNA [64, 65], which the latter is very sensitive to the mode of drug-DNA binding.

Electrostatic interaction or groove binding of complexes with DNA reveals less or no alteration on the helicity band or base stacking band but intercalators perturb both the bands [66]. As revealed in Fig. 6, by addition of the Cu(II) complex to the DNA solution, no significant changes in the form and no distinguished shift in the CD spectrum of B-DNA was recognized, which indicated that the FS-DNA kept the double helix B-form structure in the presence of Cu(II) complex. The only indicated diffrence is that by adding the complex to the DNA solution, the intensity of the both bands at 275 nm 245nm increased. The increasing of the negative peak intensity (245 nm) showed that the interaction of the complex with DNA tightened the double helix structure of DNA [67]. Thus, the possible mode of binding concluded as groove binding or electrostatic interaction.

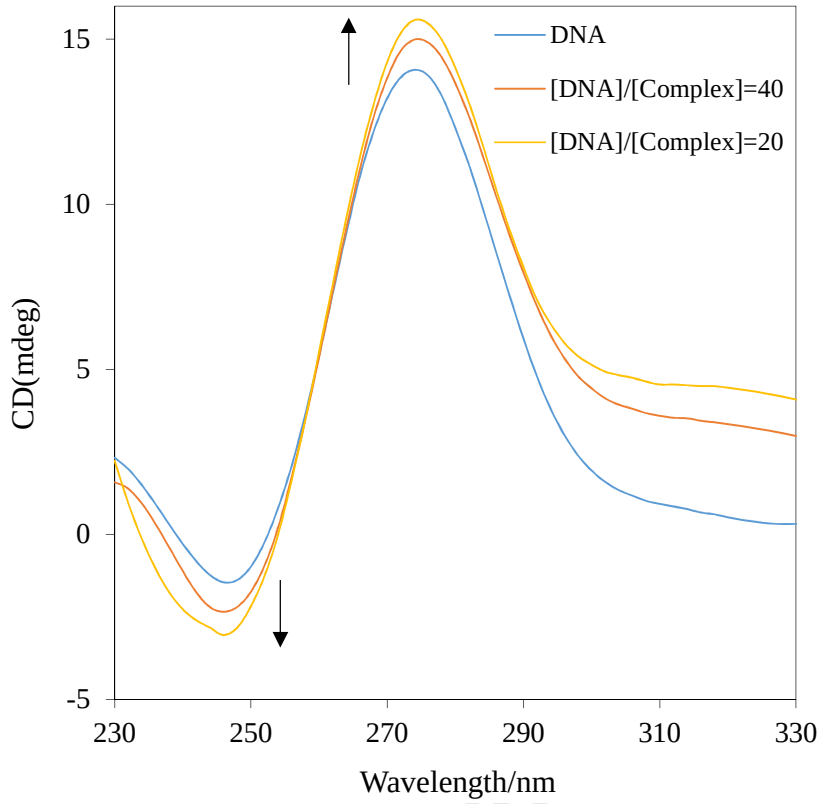

Fig. 6. The CD spectra of DNA (200μM) in the presence of complex in Tris–HCl buffer solution/0.5% DMSO. The concentrations of complex were 0, 5μM and 10μM.

Electrochemical behavior of complex in the presence of DNA. Cyclic voltammograms were run in the potential range from -1.00 to +1.00 V in DMSO (starting value: -1.00 V). The cyclic voltammograms of $[CuL]_4$ complex revealed two anodic peaks at 0.873 V, 0.373 V and two cathodic peaks at -0.024 V and -0.436 V (Fig. S16). Upon addition of DNA solution to the metal complex solution (10 mL, 10^3 μM), the anodic peaks shifted to a more positive value of 0.904 V and negative value of 0.357 V and a new anodic peak at 0.016 V appears. The cathodic peaks shifted to value that is more negative. Therefore, there is a mixed mode of binding (intercalation and groove binding) between metal complex and DNA. The observed decrease in

the anodic current and an increase in peak currents of the cathodic waves in the CV responses, suggesting the binding of the complex to the large slowly diffusing DNA molecule [68].

DNA cleavage and ethidium bromide competitive studies. The interaction between DNA and complex is important due to its effect on cell cycle arrest, gene expression modification and DNA cleavage activity. These incidences caused special programmed cell death means apoptosis. The cleavage of DNA including single or double strand cleavage caused by metal complex alone or with the cooperation of oxidant like H_2O_2 and transition metal ions like Cu^{2+}. In comparison, double strand breakage induces the most harmful damage to the cell because cellular repair systems such as NHEJ (Non-Homologous End Joining) repair the strand less accurate and with strand insertion/deletion, which cause genome instability and finally apoptosis. As an applicable method, gel electrophoresis was used to assess the structural changes induced in DNA by the Cu(II) complex. In this manner, supercoiled (SC) plasmid pBluescript KS (+) DNA was incubated with various concentrations of the complex to study their DNA cleavage ability. Agarose gel electrophoresis was used to monitor the conversion of supercoiled plasmid pBluescript KS (+) DNA (SC DNA) to the nicked circular (NC DNA) and linear open circular DNA (LC DNA). The control experiments suggested that untreated DNA (line 7 left) and untreated DNA+50 μM H_2O_2 (line 7 right) did not show any notable DNA cleavage. As shown in Fig. 7 the Cu(II) complex could not cleave DNA in physiological (PBS buffer) condition but in the presence of H_2O_2 the complex converted supercoiled (SC) DNA to nicked circular (NC) form in concentrations higher than 25 μM (Fig. 7). It may be interesting that Cu(II) complex didn't convert SC DNA to LC DNA despite the presence of aromatic moiety in the complex structure[69]. These results suggested the strong DNA cleavage activity of $[CuL]_4$ complex in the presence of H_2O_2.

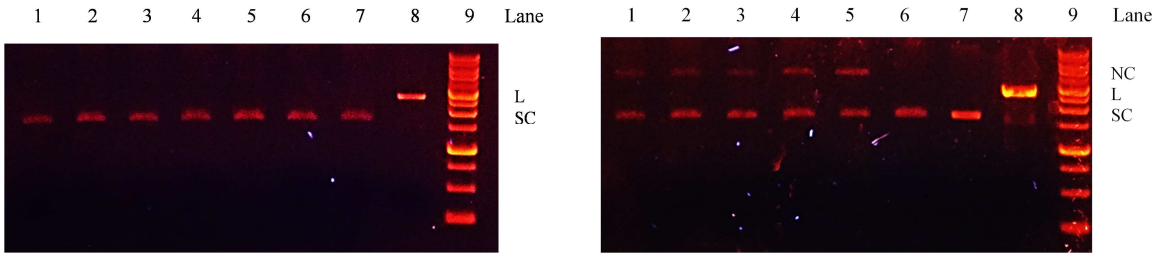

Fig. 7. Gel electrophoresis diagram of pBluescript KS (+) DNA in the presence of increasing amounts of complex 2: Left) Lane 1, DNA + 200 µM complex, Lane 2, DNA + 150 µM complex, Lane 3, DNA + 100 µM complex, Lane 4, DNA + 50 µM complex, Lane 5, DNA + 25 µM complex, Lane 6, DNA + 5 µM complex, Lane 7, DNA, Lane 8, Linear DNA (L) and Lane 9, DNA ladder. Right) Lane 1, DNA + 200 µM complex + 50 µM H_2O_2, Lane 2, DNA + 150 µM complex + 50 µM H_2O_2, Lane 3, DNA + 100 µM complex + 50 µM H_2O_2, Lane 4, DNA + 50 µM complex + 50 µM H_2O_2, Lane 5, DNA + 25 µM complex + 50 µM H_2O_2, Lane 6, DNA + 5µM complex + 50 µM H_2O_2, Lane 7, DNA + 50 µM H_2O_2, Lane 8, linear DNA and Lane 9, DNA ladder.

A famous classical double strand DNA intercalator is ethidium bromide, which can be used to further investigation on the mode of interaction. More experiments were done to assess the competitive binding affinity of EB and Cu(II) complex to DNA. HindIII digested plasmids in the presence of increasing amounts of Cu(II) complex were prepared and EB was used as a control for classic intercalation. As shown in Fig. S17, ethidium bromide displacement is not started by the complex at concentrations of 50-200 µM.

Molecular docking. One important step in drug-designing studies is molecular docking investigations. In this scaffold, locating a small molecule (complex) in the potential binding sites of a target molecule e.g. DNA is studied theoretically mainly in a non-covalent mode of binding.

Binding a small molecule to the minor groove of DNA is an important tool to recognize DNA sequence [70]. Molecular modeling allows the ligand flexibility and can calculate the minimum energy of the ligand in the active site of DNA. In this study the structure of the Cu(II) complex was obtained from the available X-ray crystallography file (cif file). The binding mode was predicted with DNA dodecamer $d(GAAGCTTC)_2$ (1Z3F). The molecular docking studies of the Cu(II) complex with DNA were performed and the energetically favorable docked pose of the complex is shown in Fig.8. The energy minimized docked pose revealed that the aromatic rings of the complex had partial intercalative interaction through π-π stacking but because of the steric hindrance of the complex, other parts of the complex could not intercalate between DNA base pairs. Therefore, groove binding better illustrated the interaction. It is worthy to note that electrostatic attraction between positive charge of Cu(II) atoms and the negative oxygen atoms of the phosphate backbone of DNA makes the binding of the complex more favourable. Also, Schiff base ligands containing N and O atoms caused Van der Waals interactions and hydrophobic contacts with DNA functional groups. The more favorable relative binding energy for the docked complex was -235.102 kcal/mol and the binding energy for all poses of the docking (Table S2) were negative (values from -192.903 to -235.102 kcal/mol for 10 poses) that indicated a high binding potential for Cu(II) complex to FS-DNA.

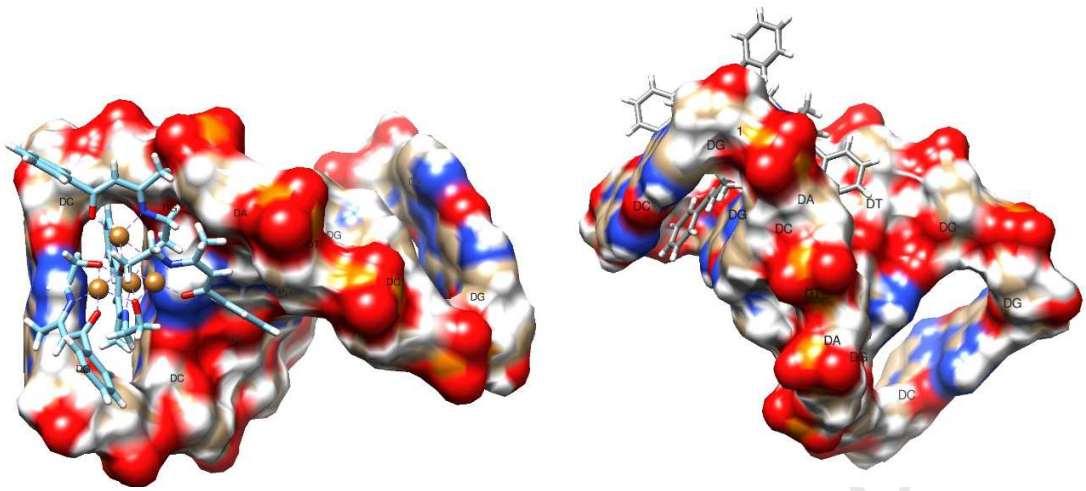

Fig. 8. Computational docking models (using the MVD software) illustrating the interactions between DNA and complex.

Protein (BSA) binding studies

General information. Often drugs exert their medicinal effect through binding to proteins and transporter proteins may help or prevent drugs from reaching their target sites [71-73]. The nature and magnitude of the binding of drugs and plasma proteins has a direct relation on drug delivery, drug absorption and the therapeutic efficiency. Therefore, investigation of proteins-metal complexes interaction is an important field for the development of new drugs and many studies have focused on the binding sites and binding modes of drug-plasma protein interactions [71].

Fluorescence quenching studies. The most abundant protein in plasma is serum albumin, which could be a potential target for many drugs to be delivered through the circulatory system. Thus considering the binding of drugs with plasma proteins is important in pharmacology and drug design. Because of the similarity of the structures of bovine serum albumin (BSA) and human serum albumin (HSA) and lower cost of BSA the most studies of the interaction with

serum albumins is performed on BSA [74]. A very sensitive and accurate method to study the interaction of drugs and protein is fluorescence spectroscopy. Using this method some useful information such as binding constant, binding mechanism, binding mode, binding sites and intermolecular distances between small-molecule substances and protein are investigated. Protein is a fluorophore and its intrinsic fluorescence is caused by three aminoacids that present in the protein structure, namely tryptophan, tyrosine, and phenylalanine residues. Intrinsic fluorescence of BSA is due essentially to Trp and Tyr aminoacids, but in most cases Phe is not excited and either its quantum yield in protein is low, so the emission from this residue is not important [74]. The fluorescence quenching could be due to different molecular interactions such as molecular rearrangements, ground state complex formation, excited-state reactions, energy transfer and collision quenching. Examining the changing in fluorescence spectra during the interaction of compounds and BSA can be used to determine a qualitative basis of analysis.

By exciting BSA at 280 nm, a strong fluorescence emission peak at 345 nm is observed. The effect of $[CuL]_4$ complex (490μM) (0-80μL) on BSA fluorescence spectra (7.2×10^{-2}μM) between 300-500 nm is shown in Fig. 9. The fluorescence emission spectra of BSA quenched by successive addition of complex along with a hypsochromic shift due to the formation of a complex between the compounds and BSA [75]. In some literatures, it is pointed that the hypsochromic shift is due to the change in microenvironment around tryptophan residues. In the other words, upon the interaction of complex with BSA, the microenvironment around tryptophan residues becomes slightly hydrophobic [76] that by considering the structure of complex it is anticipated.

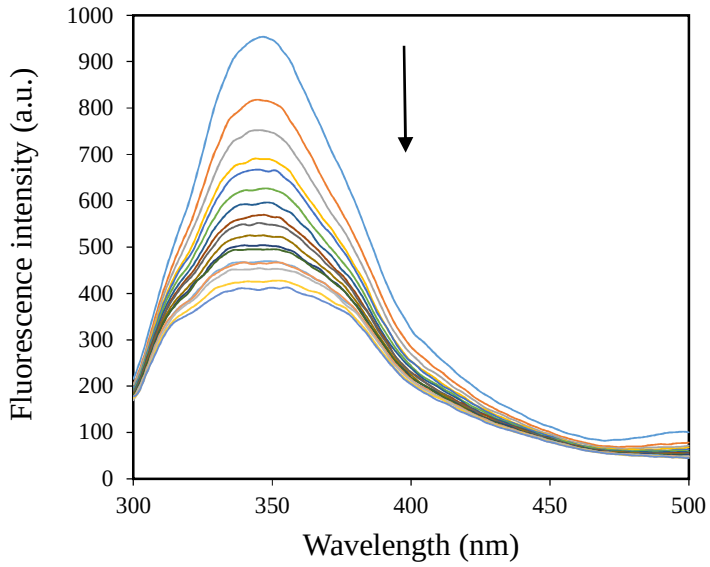

Fig. 9. Effect of $[CuL]_4$ complex (490μM) (0-80 μL) on the fluorescence spectra of BSA (7.2×10^{-2} μM) (λ_{EX} =280 nm), T=298 K

The fluorescence quenching data are analyzed by the Stern–Volmer Equation (4) [77, 78].

$$\frac{F_0}{F} = 1 + K_{SV}[Q] = 1 + k_q \tau_0 [Q] \qquad (4)$$

F denote the fluorescence intensity in the presence and F_0 in the absence of quencher. Other parameters is the Stern-Volmer quenching constant (K_{SV}), the concentration of quencher ([Q]), the bimolecular quenching constant (k_q), and the lifetime of the fluorophore in the absence of a quencher (τ_0), τ_0 is 10^{-8} s for BSA [79, 80].

From the slop of F_0/F *vs.* [Q] plot, K_{SV} value is obtained. The Stern-Volmer quenching constants K_{SV} = 7.7×10^4 M^{-1} and quenching rate constants k_q=7.7×10^{12} $M^{-1}s^{-1}$ were calculated. The linear Stern-Volmer plots showed in Fig. S18 indicated that Equation (4) is applicable for the present systems.

Fluorescence quenching occurs mainly by two mechanisms, dynamic and static quenching. Dynamic quenching refers to the excited state of the process in which the fluorophore and the quencher coming into contact and form a transition state. The static quenching refers to the ground state in which the fluorophore and quencher forming an adduct. Distinction between two types of quenching mechanism is done by UV–Vis absorption spectroscopy [81].

UV-Vis absorption studies. During the interaction between small molecules and proteins some structural changes are expected. One simple, effective and sensitive technique to monitor these changes is UV-Vis absorption spectroscopy. Normally, two main bands are the characteristics of absorption spectrum of BSA, a strong band due to the absorption of the backbone of protein which is seen around 200 nm and a weak band which is related to the absorption of amino acids (Trp, Tyr, and Phe) is seen around 278 nm [82]. Two types of quenching mentioned above are easily recognizable by UV- Vis spectral measurement. As the dynamic quenching mechanism refer to the excited state of the fluorophores so this mechanism does not affect the absorption spectra. The static quenching mechanism affects the ground-state complex formation, which results in the change of the absorption spectrum of the fluorophore [83].

Titration of BSA solution (20 µM) with increasing concentrations of the complex 0-5 µM at four temperatures (293, 298, 303 and 308K) are shown in Fig. S19. The intense band of BSA at 278nm by increasing the concentration of complex showed an increasing in the intensity without any shift which confirm a static mechanism due to the formation of an adduct between the complex and BSA in the ground state.

Equation (5) is an utilizable one for calculating the intrinsic binding constant (K_b) [84, 85]:

$$\frac{[complex]}{(\varepsilon_a - \varepsilon_f)} = \frac{[complex]}{(\varepsilon_b - \varepsilon_f)} + \frac{1}{K_b\,(\varepsilon_b - \varepsilon_f)} \qquad (5)$$

In this equation [complex] denotes the concentration of complex, ε_a the observed extinction coefficient, ε_f the extinction coefficient of the free BSA, ε_b is the extinction coefficient of the complex when fully bound to BSA, and K_b is the intrinsic binding constant. The ratio of slope to intercept in the plot of [complex]/($\varepsilon_a - \varepsilon_f$) versus [complex] gave the values of K_b (Fig. S20 and Table S3).

The different dependency of K_b values to the temperature is useful in deducing quenching mechanisms. The dynamic interaction is diffusion controlled. Increasing in temperature result in increasing the rate of diffusion and hence higher K_b obtained but increasing in temperature in the static interaction cause the dissociation of weakly bound adduct between BSA and complex in the ground state and therefore, the values of the K_b decrease [86]. The trend of K_b by increasing the temperature (Table S3) is descending which suggest a static quenching mechanism.

Thermodynamic parameters and binding modes. Similar to the other adducts in chemistry, a special interaction must exist in BSA-complex adduct formation. According to the structure of the protein, the interaction might be hydrophobic (related to the interior domains of BSA), electrostatic (related to the charge on the protein) [87], van der Waals forces or hydrogen bonding (between aminoacids and complex). The mode of binding of complex to BSA could be determined by absorption spectroscopy in different temperatures.

So for determination the binding mode the thermodynamic parameters such as free energy, enthalpy and entropy could be used for this purpose ΔH (enthalpy changes) and ΔS (entropy changes) values were calculated from van't Hoff Equation (6) [88, 89]: (Fig. S21) (Table S3)

$$\ln K_b = -\frac{\Delta H}{RT} + \frac{\Delta S}{R} \quad (6)$$

Free energy changes (ΔG) at different temperatures are calculated from Equation 7 [90, 91]:

$$\Delta G = \Delta H - T\Delta S \quad (7)$$

From the data in Table S3, negative ΔG and ΔH values confirm a spontaneous and exothermic binding process and positive ΔS value proposed an entropy-driven process. Negative ΔH and positive ΔS values suggested electrostatic mode of binding between complex and BSA according to Ross and Subramanian rules [92].

Binding stoichiometry. Generally, the native form of proteins is a three-dimensional folded conformation that is thermodynamically stable. These folded structures are stabilized by non-covalent interactions, but may become unfolded or misfolded upon binding the complex to protein because of change in non-covalent interactions. Therefore, aggregation maybe occurred between the unfolded/misfolded proteins. To determine the average aggregation number of BSA , <J>, potentially induced by the complex Equation (8) is used [93] .

$$1 - \frac{F}{F_0} = < J > \frac{[Q]}{[BSA]_0} \quad (8)$$

The slopes (<J> = 0.0019) of the line in Fig.S22 was less than unity which confirm no aggregation between protein molecules after binding the complex and a 1:1 complex-BSA stoichiometry.

Binding constants and the number of binding sites. Upon interaction of complex and BSA, the complex must find an appropriate binding site on BSA, which be unique for it. During the process a change in biological activity may occur. At the binding sites, complexes usually

form non-covalent binding completely due to their chemical structure and the strength of the chemical bond revealed the affinity of the complex to BSA. Again fluorescence spectroscopy can be useful for calculating apparent binding constant (K_b) and the number of binding sites (n) (Equation (9)) [94, 95]:

$$\log\left(\frac{F_0 - F}{F}\right) = \log K_b + n\log[Q] \qquad (9)$$

Where, K_b and [Q] are binding constant and the concentration of quencher, respectively, and n is the number of binding sites. $K_b = 4.6\times10^3\ M^{-1}$ and the number of binding sites n=0.741 were calculated (Fig. S23). The value of n is near to unity suggested only one binding site on the BSA molecule for the complex [94].

Site-selective binding of complex on BSA. Two main binding sites of bovine serum albumin for drugs are classified as site I and site II in which tryptophan residue and tyrosine residue tend to bind to small molecules, respectively. Some common site markers are used to identify the binding site of BSA e.g warfarin, phenylbutazone, etc., for site I and ibuprofen, diazepam, fluofenamic acid, etc for site II. In this study the site marker competitive experiment was done with phenylbutazone and ibuprofen for site I and site II, respectively, by preparing a solution of BSA and appropriate site marker and successive flourimetric titration by the complex solution. The results were compared with the flourimetric titration of pure BSA solution with complex. Fluorescence spectra are shown in Fig. S24, which revealed that the quenching of BSA in the presence of ibuprofen was smaller than in its absence. To facilitate the comparison of the influence of phenylbutazone and ibuprofen on the binding of the complex to BSA, in each case the binding constant values were measured (Table S4). It was revealed that the binding constant of the system decreased remarkably in the presence of ibuprofen, but a small decreasing was

observed in the presence of phenyl butazone [96, 97]. Decreasing in probe fluorescence result from competitive displacement by the complex and demonstrated the higher affinity of the complex to site II (subdomain IIIA) in BSA.

Energy transfer and binding distance between complex and BSA. To determine the approximate proximity and angular orientation of fluorophores FRET (Fluorescence resonance energy transfer) method is applied. FRET is defined as a "spectroscopic ruler" by which the distance between biological molecules is determined. In this regard the fluorescence band of one molecule (donor) overlaps with an excitation band of another (acceptor) which are within 2-8 nm [98, 99]. Some conditions must be establish for accomplishing energy transfer from donor to acceptor (1) donor must be a fluorophore to have a fluorescence band, (2) an enough overlap must be between the fluorescence spectrum of the donor and absorption spectrum of the acceptor, (3) the distance between the donor and the acceptor must be in the range 2–8 nm [100]. The distance between donor and acceptor (r) in the FRET method is calculated by Equation (10):

$$E = \frac{R_0^6}{R_0^6 + r^6} = 1 - \frac{F}{F_0} \qquad (10)$$

Where E is the transfer efficiency between donor and acceptor, F and F_0 are the fluorescence intensities of BSA in the presence and absence of complex, r is the donor–acceptor distance and R_0 (calculated from Equation 11) is the critical distance where the transfer efficiency is 50%:

$$R_0^6 = 8.8 \times 10^{-25} K^2 N^{-4} \Phi J \qquad (11)$$

The value of K^2 = 2/3 is used for random orientation of the donor and acceptor in fluid solution, N is the averaged refracted index of the medium in the wavelength range where spectral overlap is significant, and N= 1.336 for the average refracted index of water and organics, Φ is

the fluorescence quantum yield of the donor, that Φ = 0.118 for the fluorescence quantum yield of tryptophan [100], J is the effect of the spectral overlap between the emission spectrum of the donor and the absorption spectrum of the acceptor, which could be calculated by Equation 12:

$$J = \frac{\int_0^\infty F(\lambda)\varepsilon(\lambda)\lambda^4 d\lambda}{\int_0^\infty F(\lambda)d\lambda} \qquad (12)$$

In this equation F(λ) is the corrected fluorescence intensity of the donor in the wavelength range from λ to (l+Δλ) and ε(λ) is the molar extinction coefficient of the acceptor at λ.

The overlap of BSA emission spectrum and the complex absorption spectrum is the basis of FRET that regarding to Fig. S25 it has a considerable amount. Thus, FRET theory is applicable to determine the distance between the amino acid residues on protein and the complex in the binding site [101]. According to Equations 10, 11, 12, the values of E= 0.57, J = 1.83×10^{-15} cm^3 L mol^{-1}, R_0 = 1.90 nm and the binding distance r = 1.81 nm were calculated. The value of r is less than 8 nm, and $0.5R_0 < r < 1.5R_0$, indicating the energy transfer from BSA to the complex occurs with high probability [102-104].

Synchronous fluorescence spectroscopic studies. The intrinsic fluorescence of BSA is mainly due to emission of tyrosine and tryptophan residues. Therefore, it is reasonable that the emission spectrum of BSA be sensitive to the microenvironment of these chromophores. Synchronous fluorescence experiments effectively reveals the mentioned conformational changes in BSA sites upon interaction with complex [105]. Synchronous fluorescence spectra were achieved by maintaining a known constant wavelength difference which derive from the difference between excitation and emission wavelengths ($\Delta\lambda = \lambda_{em} - \lambda_{ex}$) of chromophores namely tryptophan and tyrosine. The large Δλ = 60 nm and small Δλ = 15 nm values for BSA

system are ascribed to the fluorescence of tryptophan and tyrosine residue, respectively [106, 107]. The maximum of the emission spectra of BSA which mainly result from the tryptophan and tyrosine residues can be straightforward related to the polarity of their surroundings [105]. in this regard, increasing in the polarity of the surrounding environment, decreasing in hydrophobicity and losing the structure of BSA, cause a shift of the maximum emission wavelength [100, 108].

The addition of various concentrations of the complex to the synchronous fluorescence spectrum of BSA at $\Delta\lambda$=15 (Fig. S26 (a)), revealed a small quenching, with 1 - 2 nm shift in the maximum of peak (282nm) within the applied concentration range. Therefore, the effect of complex on the microenvironment of the tyrosine residue was very little and could be ignored. The synchronous fluorescence spectra of BSA at $\Delta\lambda$=60 nm exhibited more intense quenching (Fig. S26 (b)) at 280 nm with 1 - 2 nm shift in the position of the band. It indicated that the conformation of BSA was changed because of increasing the polarity and decreasing the hydrophobicity of the microenvironment around tryptophan residue [100]. Therefore, it further confirmed that the complex bound to site II of BSA.

Circular dichroism spectroscopy. CD spectroscopy is an important technique for structure characterization of proteins [109]. The CD spectra of BSA in the absence and presence of the complex is shown in Fig 10. Upon addition of the complex, α-helix decrease from 64% (free BSA) to 29%, and a slight increase in turn from 13% (free BSA) to 16% along with a dramatic increase of random coil from 16% to 37% was observed (Table. S5). Thus, some α-helix converted into random coil and turn structures when BSA was conjugated with the complex.

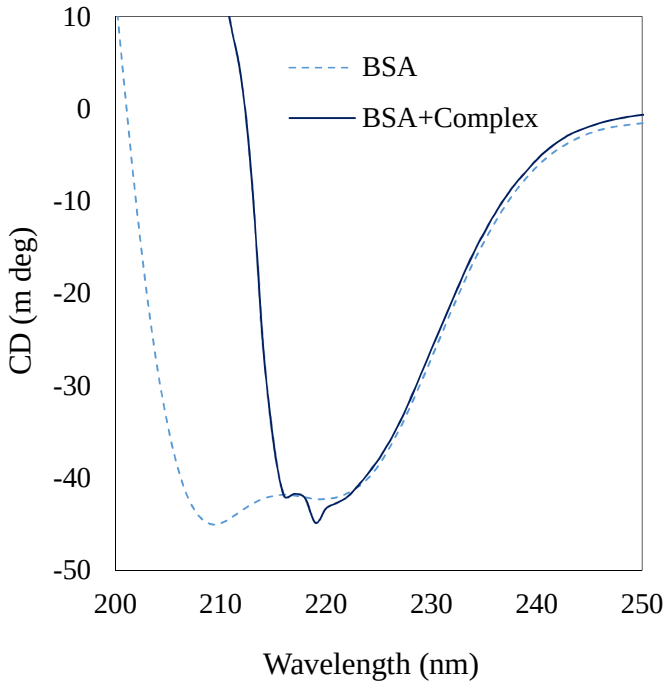

Fig. 10. CD spectra of the BSA (4µM) in the absence and presence of the complex (4µM) in Tris buffer (pH 7.2) containing 0.4 % DMSO.

Molecular docking study. The BSA molecule is made up of three homologous domains: domain I (residues 1–195), II (196–383) and III (384–585) that are divided into nine loops (L1–L9) by 17 disulfide bridges. Each domain is composed of two sub-domains (A and B) (Fig. S27) [110].

In the present study, the MVD program [111] was chosen to obtain the binding mode of the complex at the active site of BSA. The ranked results are reported in Table S6 and the best-ranked result was obtained for site II of BSA. As shown in Fig. S28a, the complex is inserted into the hydrophobic residues of site II (subdomain IIIA). The binding energy for the complex to BSA was found to be −154.82. These results are in agreement with those obtained by the experimental method. Fig. S28b shows that the complex is surrounded by amino acid residues

such as: Thr448, Pro383, Leu452, Arg484, Pro485, Glu382, Ser488, Ala489, Lys413, Leu490, Thr491, Pro492, Arg409, Leu386, Asn390, Ile387, Asn385, Gln389.

Anticancer activity studies

Studies on the anticancer properties of metal Schiff base complexes have been of considerable attention [112-115]. We measured the anticancer activity of the complex against Jurkat, Raji and A549 cell lines using MTT assay. Cell lines were treated with increasing concentrations of the complex for 48 h, and then the level of cytotoxicity was quantified. As shown in Fig. S29 the complex had cytotoxic effects against all tested cell lines. To compare the cytotoxic activity of the complex on various cell lines, the IC_{50} values were determined. Table S7 demonstrates that the IC_{50} values of the complex for Jurkat (20.3 μg/mL) and Ragi (23.1 μg/mL) cell lines (<0.23 μg/mL) were slightly lower than that for A549 cell line (29.2 μg/mL) showed a slightly more effectiveness of the complex on cells of leukemia origin. The IC_{50} values of the complex for each cell line were also comparable to that of *cis-platin* (25 μg/mL for Jurkat, 30 μg/mL for Raji and 79.4 μg/mL for A549 cells).

Conclusion

In the present study, we have reported for the first time that a tridentate Schiff base ligand could be used to produce a novel Cu(II) distorted cubane complex containing a Cu_4O_4 core. We have also shown that the tetra-nuclear Cu(II) cubane complex $[CuL]_4$ can act as an efficient catalyst in the temperature dependent oxidation of 3,5-ditertbutylcatechol to its corresponding o-quinone. The kinetics of the oxidation were studied under pseudo first order condition at four different temperatures from 283 to 313K. The positive free energy leads to a nonspontaneous process. In addition, the positive $\Delta H^{\#}$ (activation enthalpy changes) values confirmed

endothermic process and the proposed catalytic cycle of the process clearly explained the positive value of $\Delta S^{\#}$ (activation entropy changes).

The cubane complex was further investigated in DNA & BSA binding, DNA cleavage and anticancer activity. The results revealed that the main mode of binding of the complex to FS-DNA was intercalation. Gel electrophoresis studies suggested the strong DNA cleavage activity of $[CuL]_4$ complex in the presence of H_2O_2. The complex exhibited excellent binding affinity to BSA without any aggregation for the albumin molecule. Competitive experiments revealed that site II of BSA was suitable to accommodate the complex. The results of synchronous fluorescence showed that the conformation of BSA was changed because of an increase in the polarity and decrease in the hydrophobicity of the microenvironment around tryptophan residue, which further confirmed site II of BSA for binding. Considering the negative ΔH and positive ΔS values, thermodynamic results suggested electrostatic mode of binding between the complex and BSA. The values of K_b decreased with increasing temperature, which suggests a static mechanism. The theoretical docking studies were performed both for DNA & for BSA bindings.

Finally, the complex was screened for its anticancer activity against Jurkat human T cell leukemia, Raji Burkitt's lymphoma and A549 lung carcinoma cell lines, which revealed that the $[CuL]_4$ complex has better anticancer activity than *cis-platin*.

Acknowledgements

We are grateful to the Shiraz university research council for its financial support. The crystallographic part was supported by the project 18-10504S of the Czech Science Foundation using instruments of the ASTRA lab established within the Operation program Prague Competitiveness - project CZ.2.16/3.1.00/24510.

Supplementary material

CCDC 1851488 contains the supplementary crystallographic data for this paper. These data can be obtained free of charge from The Cambridge Crystallographic Data Centre via www.ccdc.cam.ac.uk/data_request/cif.

References

1. Majumder S, Sarkar S, Sasmal S, Sãnudo EC, Mohanta S. Heterobridged dinuclear, tetranuclear, dinuclear-based 1-D, and heptanuclear-based 1-D complexes of copper (II) derived from a dinucleating ligand: syntheses, structures, magnetochemistry, spectroscopy, and catecholase activity. Inorg Chem. 2011;50(16):7540-54.
2. Yang CT, Moubaraki B, Murray KS, Ranford JD, Vittal JJ. Interconversion of a Monomer and Two Coordination Polymers of a Copper (II)− Reduced Schiff Base Ligand− 1, 10-Phenanthroline Complex Based on Hydrogen-and Coordinative-Bonding. Inorg Chem. 2001;40(23):5934-41.
3. Mergehenn R, Haase W. The crystal structure of cyanato (2-dimethylaminoethanolato) copper (II), C5H10N2O2Cu. Acta Crystallographica Section B. 1977;33(6):1877-82.
4. Ruiz E, Rodríguez-Fortea A, Alemany P, Alvarez S. Density functional study of the exchange coupling in distorted cubane complexes containing the Cu4O4 core. Polyhedron. 2001;20(11-14):1323-7.
5. Zhang J, Wojtas L, Larsen RW, Eddaoudi M, Zaworotko MJ. Temperature and concentration control over interpenetration in a metal− organic material. JACS. 2009;131(47):17040-1.
6. Nayak M, Jana A, Fleck M, Hazra S, Mohanta S. A unique example of a three component cocrystal of metal complexes. CrystEngComm. 2010;12(5):1416-21.
7. Das K, Mondal TK, Garribba E, Fondo M, Sinha C, Datta A. Phenoxo bridged tetranuclear copper (II) and dinuclear zinc (II) complexes of 2, 6-diformyl-4-methylphenol-di (benzoylhydrazone): Synthesis, structure, spectra and magnetism. Inorg Chim Acta. 2014;413:194-202.
8. Wang H, Zhang D, Chen Y, Ni Z-H, Tian L, Jiang J. Synthesis, crystal structures, and magnetic properties of new tetranuclear Cu (II) complexes of bis-bidentate Schiff-base ligands. Inorg Chim Acta. 2009;362(14):4972-6.
9. Senthil Raja D, Bhuvanesh NS, Natarajan K. Effect of N (4)-phenyl substitution in 2-oxo-1, 2-dihydroquinoline-3-carbaldehyde semicarbazones on the structure, DNA/protein interaction, and antioxidative and cytotoxic activity of Cu (II) complexes. Inorg Chem. 2011;50(24):12852-66.
10. Koval IA, Gamez P, Belle C, Selmeczi K, Reedijk J. Synthetic models of the active site of catechol oxidase: mechanistic studies. Chem Soc Rev. 2006;35(9):814-40.
11. Smith SJ, Noble CJ, Palmer RC, Hanson GR, Schenk G, Gahan LR, et al. Structural and spectroscopic studies of a model for catechol oxidase. J Biol Inorg Chem. 2008;13(4):499-510.

12. Majumder A, Goswami S, Batten SR, El Fallah MS, Ribas J, Mitra S. Catalytic oxidation of 3, 5-di-tert-butylcatechol by a manganese (III) 18-azametallacrown-6 compound: Synthesis, crystal structure, fluorescence, magnetic and kinetic investigation. Inorg Chim Acta. 2006;359(8):2375-82.
13. Rey NA, Neves A, Bortoluzzi AJ, Pich CT, Terenzi H. Catalytic promiscuity in biomimetic systems: catecholase-like activity, phosphatase-like activity, and hydrolytic DNA cleavage promoted by a new dicopper (II) hydroxo-bridged complex. Inorg Chem. 2007;46(2):348-50.
14. Boulikas T, Vougiouka M. Cisplatin and platinum drugs at the molecular level. Oncol Rep. 2003;10(6):1663-82.
15. Wong E, Giandomenico CM. Current status of platinum-based antitumor drugs. Chem Rev. 1999;99(9):2451-66.
16. Jamieson ER, Lippard SJ. Structure, recognition, and processing of cisplatin− DNA adducts. Chem Rev. 1999;99(9):2467-98.
17. Wang D, Lippard SJ. Cellular processing of platinum anticancer drugs. Nat Rev Drug discovery. 2005;4(4):307.
18. Rajendiran V, Karthik R, Palaniandavar M, Stoeckli-Evans H, Periasamy VS, Akbarsha MA, et al. Mixed-ligand copper (II)-phenolate complexes: effect of coligand on enhanced DNA and protein binding, DNA cleavage, and anticancer activity. Inorg Chem. 2007;46(20):8208-21.
19. Bhat SS, Kumbhar AA, Heptullah H, Khan AA, Gobre VV, Gejji SP, et al. Synthesis, electronic structure, DNA and protein binding, DNA cleavage, and anticancer activity of fluorophore-labeled copper (II) complexes. Inorg Chem. 2010;50(2):545-58.
20. Primik MF, Göschl S, Jakupec MA, Roller A, Keppler BK, Arion VB. Structure− Activity Relationships of Highly Cytotoxic Copper (II) Complexes with Modified Indolo [3, 2-c] quinoline Ligands. Inorg Chem. 2010;49(23):11084-95.
21. Krishnamoorthy P, Sathyadevi P, Cowley AH, Butorac RR, Dharmaraj N. Evaluation of DNA binding, DNA cleavage, protein binding and in vitro cytotoxic activities of bivalent transition metal hydrazone complexes. Eur J Med Chem. 2011;46(8):3376-87.
22. Hegg EL, Burstyn JN. Toward the development of metal-based synthetic nucleases and peptidases: a rationale and progress report in applying the principles of coordination chemistry. Coord Chem Rev. 1998;173(1):133-65.
23. Dhar S, Senapati D, Das PK, Chattopadhyay P, Nethaji M, Chakravarty AR. Ternary copper complexes for photocleavage of DNA by red light: Direct Evidence for sulfur-to-copper charge transfer and d− d band involvement. JACS. 2003;125(40):12118-24.
24. Sielecki TM, Boylan JF, Benfield PA, Trainor GL. Cyclin-dependent kinase inhibitors: useful targets in cell cycle regulation. J Med Chem. 2000;43(1):1-18.
25. Zhang Z, Jin L, Qian X, Wei M, Wang Y, Wang J, et al. Novel Bcl-2 inhibitors: discovery and mechanism study of small organic apoptosis-inducing agents. ChemBioChem. 2007;8(1):113-21.
26. Siu PK-M, Ma D-L, Che C-M. Luminescent cyclometalated platinum (II) complexes with amino acid ligands for protein binding. Chem Commun. 2005(8):1025-7.
27. Reim J, Krebs B. Synthesis, structure and catecholase activity study of dinuclear copper (II) complexes. Dalton Trans. 1997(20):3793-804.
28. Neves A, Rossi LM, Bortoluzzi AJ, Szpoganicz B, Wiezbicki C, Schwingel E, et al. Catecholase Activity of a Series of Dicopper (II) Complexes with Variable Cu− OH (phenol) Moieties. Inorg Chem. 2002;41(7):1788-94.

29. Oishi N, Nishida Y, Ida K, Kida S. Reaction between various copper (II) complexes and ascorbic acid or 3, 5-di-t-butylcatechol. Bull Chem Soc Jpn. 1980;53(10):2847-50.
30. Palatinus L, Chapuis G. SUPERFLIP–a computer program for the solution of crystal structures by charge flipping in arbitrary dimensions. J Appl Crystallogr. 2007;40(4):786-90.
31. Petříček V, Dušek M, Palatinus L. Crystallographic computing system JANA2006: general features. Z Kristallog – Cryst Mater. 2014;229(5):345-52.
32. Amirghofran Z, Bahmani M, Azadmehr A, Javidnia K. Anticancer effects of various Iranian native medicinal plants on human tumor cell lines. Neoplasma. 2006;53(5):428-33.
33. West DX, Nassar AA, El-Saied FA, Ayad MI. Cobalt (II) complexes with 2-aminoacetophenone N (4)-substituted thiosemicarbazones. Transition Metal Chemistry. 1999;24(6):617-21.
34. Tümer M, Köksal H, Sener MK, Serin S. Antimicrobial activity studies of the binuclear metal complexes derived from tridentate Schiff base ligands. Transition Metal Chemistry. 1999;24(4):414-20.
35. Meghdadi S, Mereiter K, Langer V, Amiri A, Erami RS, Alshima'a AM, et al. Synthesis, X-ray crystal structure, and electrochemistry of copper (II) complexes of a new tridentate unsymmetrical Schiff base ligand and its hydrolytically rearranged isomer. Inorganica Chimica Acta. 2012;385:31-8.
36. Gordon A, Ford R. A Chemists Companion: A Handbook of Practical Data, Techniques, and References, Wiley Interscience. 1972.
37. Mohamed GG, El-Wahab ZHA. Mixed ligand complexes of bis (phenylimine) Schiff base ligands incorporating pyridinium moiety: Synthesis, characterization and antibacterial activity. Spectrochimica Acta Part A: Molecular and Biomolecular Spectroscopy. 2005;61(6):1059-68.
38. Zhang Y-L, Ruan W-J, Zhao X-J, Wang H-G, Zhu Z-A. Synthesis and characterization of axial coordination cobalt (III) complexes containing chiral Salen ligands. Polyhedron. 2003;22(12):1535-45.
39. Deacon G, Phillips R. Relationships between the carbon-oxygen stretching frequencies of carboxylato complexes and the type of carboxylate coordination. Coordination Chemistry Reviews. 1980;33(3):227-50.
40. Nakamoto K. Infrared and Raman spectra of inorganic and coordination compounds. 1978.
41. Felicio R, Cavalheiro E, Dockal E. Preparation, characterization and thermogravimetric studies of [N, N′-cis-1, 2-cyclohexylene bis (salicylideneaminato)] cobalt (II) and [N, N′-(±)-trans-1, 2-cyclo-hexylene bis (salicylideneaminato)] cobalt (II). Polyhedron. 2001;20(3-4):261-8.
42. Zolezzi S, Decinti A, Spodine E. Syntheses and characterization of copper (II) complexes with Schiff-base ligands derived from ethylenediamine, diphenylethylenediamine and nitro, bromo and methoxy salicylaldehyde. Polyhedron. 1999;18(6):897-904.
43. Ghose B, Lasisi K. Schiff Base Complexes of Titanium: Reaction of Titanium (IV) Tetrachloride with Dibasic Tetradentate Schiff Bases. Synthesis and Reactivity in Inorganic and Metal-Organic Chemistry. 1986;16(8):1121-33.
44. Ribas J, Diaz C, Costa R, Journaux Y, Mathoniere C, Kahn O, et al. Structure and magnetic and spectroscopic properties of a nickelIIcopperIInickelII trinuclear species. Inorganic Chemistry. 1990;29(11):2042-7.
45. Addison AW, Rao TN, Reedijk J, van Rijn J, Verschoor GC. Synthesis, structure, and spectroscopic properties of copper (II) compounds containing nitrogen–sulphur donor ligands;

the crystal and molecular structure of aqua [1, 7-bis (N-methylbenzimidazol-2′-yl)-2, 6-dithiaheptane] copper (II) perchlorate. J Chem Soc, Dalton Trans. 1984(7):1349-56.
46. Monzani E, Battaini G, Perotti A, Casella L, Gullotti M, Santagostini L, et al. Mechanistic, structural, and spectroscopic studies on the catecholase activity of a dinuclear copper complex by dioxygen. Inorg Chem. 1999;38(23):5359-69.
47. Selmeczi K, Réglier M, Giorgi M, Speier G. Catechol oxidase activity of dicopper complexes with N-donor ligands. Coord Chem Rev. 2003;245(1-2):191-201.
48. Banu KS, Chattopadhyay T, Banerjee A, Mukherjee M, Bhattacharya S, Patra GK, et al. Mono-and dinuclear manganese (III) complexes showing efficient catechol oxidase activity: syntheses, characterization and spectroscopic studies. Dalton Trans. 2009(40):8755-64.
49. Jaumot J, Gargallo R. Experimental methods for studying the interactions between G-quadruplex structures and ligands. Curr Pharm Des. 2012;18(14):1900-16.
50. Bhat SS, Kumbhar AA, Heptullah H, Khan AA, Gobre VV, Gejji SP, et al. Synthesis, electronic structure, DNA and protein binding, DNA cleavage, and anticancer activity of fluorophore-labeled copper (II) complexes. Inorg Chem. 2010;50(2):545-58.
51. Sirajuddin M, Ali S, Haider A, Shah NA, Shah A, Khan MR. Synthesis, characterization, biological screenings and interaction with calf thymus DNA as well as electrochemical studies of adducts formed by azomethine [2-((3, 5-dimethylphenylimino) methyl) phenol] and organotin (IV) chlorides. Polyhedron. 2012;40(1):19-31.
52. Sirajuddin M, Ali S, Shah NA, Khan MR, Tahir MN. Synthesis, characterization, biological screenings and interaction with calf thymus DNA of a novel azomethine 3-((3, 5-dimethylphenylimino) methyl) benzene-1, 2-diol. Spectrochim Acta, Part A. 2012;94:134-42.
53. Carter MT, Rodriguez M, Bard AJ. Voltammetric studies of the interaction of metal chelates with DNA. 2. Tris-chelated complexes of cobalt (III) and iron (II) with 1, 10-phenanthroline and 2, 2'-bipyridine. J Am Chem Soc. 1989;111(24):8901-11.
54. Zarei L, Asadi Z, Dusek M, Eigner V. Homodinuclear Ni (II) and Cu (II) Schiff base complexes derived from O-vanillin with a pyrazole bridge: Preparation, crystal structures, DNA and protein (BSA) binding, DNA cleavage, molecular docking and cytotoxicity study. J Photochem Photobiol, A. 2019;374:145-60.
55. Dimiza F, Perdih F, Tangoulis V, Turel I, Kessissoglou DP, Psomas G. Interaction of copper (II) with the non-steroidal anti-inflammatory drugs naproxen and diclofenac: Synthesis, structure, DNA-and albumin-binding. J Inorg Biochem. 2011;105(3):476-89.
56. Selvakumar B, Rajendiran V, Maheswari PU, Stoeckli-Evans H, Palaniandavar M. Structures, spectra, and DNA-binding properties of mixed ligand copper (II) complexes of iminodiacetic acid: The novel role of diimine co-ligands on DNA conformation and hydrolytic and oxidative double strand DNA cleavage. J Inorg Biochem. 2006;100(3):316-30.
57. Waring M. Complex formation between ethidium bromide and nucleic acids. J Mol Biol. 1965;13(1):269-82.
58. Kelly JM, Tossi AB, McConnell DJ, OhUigin C. A study of the interactions of some polypyridylruthenium (II) complexes with DNA using fluorescence spectroscopy, topoisomerisation and thermal denaturation. Nucleic Acids Res. 1985;13(17):6017-34.
59. Liu J, Zhang H, Chen C, Deng H, Lu T, Ji L. Interaction of macrocyclic copper (II) complexes with calf thymus DNA: effects of the side chains of the ligands on the DNA-binding behaviors. Dalton Trans. 2003(1):114-9.

60. Barmpa A, Frousiou O, Kalogiannis S, Perdih F, Turel I, Psomas G. Manganese (II) complexes of the quinolone family member flumequine: Structure, antimicrobial activity and affinity for albumins and calf-thymus DNA. Polyhedron. 2018;145:166-75.
61. Sirajuddin M, Ali S, Badshah A. Drug–DNA interactions and their study by UV–Visible, fluorescence spectroscopies and cyclic voltametry. J Photochem Photobiol, B. 2013;124:1-19.
62. Baguley BC, Le Bret M. Quenching of DNA-ethidium fluorescence by amsacrine and other antitumor agents: a possible electron-transfer effect. Biochemistry. 1984;23(5):937-43.
63. Mariappan M, Alagarsamy R, Panneerselvam AP, Veerappan A, Rajendran S, Arunachalam J. Synthesis, solvatochromism, photochemistry, DNA binding, photocleavage, cytotoxicity and molecular docking studies of a ruthenium (II) complex bearing photoactive subunit. J Photochem Photobiol, A. 2018;356:617-26.
64. Mahadevan S, Palaniandavar M. Spectral and electrochemical behavior of copper (ii)− phenanthrolines bound to calf thymus DNA.[(5, 6-dimethyl-OP) 2Cu] 2+(5, 6-dimethyl-OP= 5, 6-dimethyl-1, 10-phenanthroline) induces a conformational transition from B to Z DNA. Inorg Chem. 1998;37(16):3927-34.
65. Xu Z-H, Chen F-J, Xi P-X, Liu X-H, Zeng Z-Z. Synthesis, characterization, and DNA-binding properties of the cobalt (II) and nickel (II) complexes with salicylaldehyde 2-phenylquinoline-4-carboylhydrazone. J Photochem Photobiol, A. 2008;196(1):77-83.
66. Sarwar T, Rehman SU, Husain MA, Ishqi HM, Tabish M. Interaction of coumarin with calf thymus DNA: deciphering the mode of binding by in vitro studies. Int J Biol Macromol. 2015;73:9-16.
67. Li H, Bu X, Lu J, Xu C, Wang X, Yang X. Interaction study of ciprofloxacin with human telomeric DNA by spectroscopy and molecular docking. Spectrochim Acta, Part A. 2013;107:227-34.
68. Arshad N, Farooqi SI. Cyclic Voltammetric DNA Binding Investigations on Some Anticancer Potential Metal Complexes: a Review. Appl Biochem Biotechnol. 2018:1-21.
69. Sundaravadivel E, Vedavalli S, Kandaswamy M, Varghese B, Madankumar P. DNA/BSA binding, DNA cleavage and electrochemical properties of new multidentate copper (II) complexes. RSC Advances. 2014;4(77):40763-75.
70. Zheng K, Zhu L, Li Y-T, Wu Z-Y, Yan C-W. Synthesis and crystal structure of new dicopper (II) complexes having asymmetric N, N′-bis (substituted) oxamides with DNA/protein binding ability: In vitro anticancer activity and molecular docking studies. J Photochem Photobiol B, Biol. 2015;149:129-42.
71. Wang W, Gan N, Sun Q, Wu D, Gan R, Zhang M, et al. Study on the interaction of ertugliflozin with human serum albumin in vitro by multispectroscopic methods, molecular docking, and molecular dynamics simulation. Spectrochim Acta, Part A. 2019;219:83-90.
72. Ma R, Guo D-X, Li H-F, Liu H-X, Zhang Y-R, Ji J-B, et al. Spectroscopic methodologies and molecular docking studies on the interaction of antimalarial drug piperaquine and its metabolites with human serum albumin. Spectrochim Acta, Part A. 2019:117158.
73. Morales-Toyo M, Glidewell C, Bruno-Colmenares J, Cubillán N, Sánchez-Colls R, Alvarado Y, et al. Synthesis of (E)-Ethyl-4-(2-(furan-2-ylmethylene) hydrazinyl) benzoate, crystal structure, and studies of its interactions with human serum albumin by spectroscopic fluorescence and molecular docking methods. Spectrochim Acta, Part A. 2019;216:375-84.
74. Shokohi-Pour Z, Chiniforoshan H, Sabzalian MR, Esmaeili S-A, Momtazi-borojeni AA. Cobalt (II) complex with novel unsymmetrical tetradentate Schiff base (ON) ligand: in vitro

cytotoxicity studies of complex, interaction with DNA/protein, molecular docking studies, and antibacterial activity. J Biomol Struct Dyn. 2018;36(2):532-49.
75. Poureshghi F, Ghandforoushan P, Safarnejad A, Soltani S. Interaction of an antiepileptic drug, lamotrigine with human serum albumin (HSA): Application of spectroscopic techniques and molecular modeling methods. J Photochem Photobiol, B. 2017;166:187-92.
76. Dey G, Gaur P, Giri R, Ghosh S. Optical signaling in biofluids: a nondenaturing photostable molecular probe for serum albumins. Chem Commun 2016;52(9):1887-90.
77. Sun Y, Wei S, Yin C, Liu L, Hu C, Zhao Y, et al. Synthesis and spectroscopic characterization of 4-butoxyethoxy-N-octadecyl-1, 8-naphthalimide as a new fluorescent probe for the determination of proteins. Bioorg Med Chem Lett. 2011;21(12):3798-804.
78. Zhao X, Sheng F, Zheng J, Liu R. Composition and stability of anthocyanins from purple Solanum tuberosum and their protective influence on Cr (VI) targeted to bovine serum albumin. J Agric Food Chem. 2011;59(14):7902-9.
79. Tian J, Liu X, Zhao Y, Zhao S. Studies on the interaction between tetraphenylporphyrin compounds and bovine serum albumin. J Lumin. 2007;22(5):446-54.
80. Zhao X, Hao F, Lu D, Liu W, Zhou Q, Jiang G. Influence of the surface functional group density on the carbon-nanotube-induced α-chymotrypsin structure and activity alterations. ACS Appl Mater Interfaces. 2015;7(33):18880-90.
81. Naseri A, Hosseini S, Rasoulzadeh F, Rashidi M-R, Zakery M, Khayamian T. Interaction of norfloxacin with bovine serum albumin studied by different spectrometric methods; displacement studies, molecular modeling and chemometrics approaches. J Lumin. 2015;157:104-12.
82. Chaturvedi SK, Ahmad E, Khan JM, Alam P, Ishtikhar M, Khan RH. Elucidating the interaction of limonene with bovine serum albumin: a multi-technique approach. Molecular BioSystems. 2015;11(1):307-16.
83. Kalaivani P, Prabhakaran R, Kaveri M, Huang R, Staples R, Natarajan K. Synthesis, spectral, X-ray crystallography, electrochemistry, DNA/protein binding and radical scavenging activity of new palladium (II) complexes containing triphenylarsine. Inorg Chim Acta. 2013;405:415-26.
84. Devagi G, Dallemer F, Kalaivani P, Prabhakaran R. Organometallic ruthenium (II) complexes containing NS donor Schiff bases: Synthesis, structure, electrochemistry, DNA/BSA binding, DNA cleavage, radical scavenging and antibacterial activities. J Organomet Chem. 2018;854:1-14.
85. Tikhomirova AA, Tcyrulnikov NA, Wilson RM. Synthesis, Characterization, DNA Binding and Cleaving Properties of Photochemically Activated Phenanthrene Dihydrodioxin. J Photochem Photobiol, A. 2019.
86. Asadi Z, Golchin M, Eigner V, Dusek M, Amirghofran Z. A novel water-soluble tetranuclear copper (II) Schiff base cluster bridged by 2, 6-bis-[(2-hydroxyethylimino) methyl]-4-methylphenol in interaction with BSA: Synthesis, X-ray crystallography, docking and cytotoxicity studies. J Photochem Photobiol, A. 2018;361:93-104.
87. Wilkins RG. Kinetics and mechanisms of reactions of transition metal complexes: VCH Publishers; 1991.
88. Patel R, Mir MUH, Maurya JK, Singh UK, Maurya N, Parray Mud, et al. Spectroscopic and molecular modelling analysis of the interaction between ethane-1, 2-diyl bis (N, N-dimethyl-N-hexadecylammoniumacetoxy) dichloride and bovine serum albumin. Luminescence. 2015;30(8):1233-41.

89. Zhang YZ, Chen XX, Dai J, Zhang XP, Liu YX, Liu Y. Spectroscopic studies on the interaction of lanthanum (III) 2-oxo-propionic acid salicyloyl hydrazone complex with bovine serum albumin. Luminescence. 2008;23(3):150-6.
90. Wang N, Ye L, Yan F, Xu R. Spectroscopic studies on the interaction of azelnidipine with bovine serum albumin. Int J Pharm. 2008;351(1-2):55-60.
91. Xu C, Zhao X, Wang L, Zhang X, Wang Y, Lan J. Protein Conjugation with Gold Nanoparticles: Spectroscopic and Thermodynamic Analysis on the Conformational and Activity of Serum Albumin. J Nanosci Nanotechnol. 2018;18(11):7818-23.
92. Safarnejad A, Shaghaghi M, Dehghan G, Soltani S. Binding of carvedilol to serum albumins investigated by multi-spectroscopic and molecular modeling methods. J Lumin. 2016;176:149-58.
93. Asadi Z, Haddadi E, Sedaghat M. Substitution of PPh3+ as a lipophilic cation on new water-soluble Co (II) and Zn (II) Schiff base complexes: Effect of central metal and substitutional group of ligand on DNA-complex interaction. J Photochem Photobiol, A. 2017;337:140-50.
94. Singh N, Pagariya D, Jain S, Naik S, Kishore N. Interaction of copper (II) complexes by bovine serum albumin: spectroscopic and calorimetric insights. J Biomol Struct Dyn. 2018;36(9):2449-62.
95. Zhao X, Liu R, Teng Y, Liu X. The interaction between Ag+ and bovine serum albumin: a spectroscopic investigation. Sci Total Environ 2011;409(5):892-7.
96. Zhang Y, Shi S, Chen X, Zhang W, Huang K, Peng M. Investigation on the interaction between ilaprazole and bovine serum albumin without or with different C-ring flavonoids from the viewpoint of food–drug interference. Journal of agricultural and food chemistry. 2011;59(15):8499-506.
97. Hu Y-J, Ou-Yang Y, Dai C-M, Liu Y, Xiao X-H. Site-selective binding of human serum albumin by palmatine: spectroscopic approach. Biomacromolecules. 2009;11(1):106-12.
98. Bano S, Mohd A, Khan AAP, Siddiqi K. Complexation and mechanism of fluorescence quenching of telmisartan with Y (III) and Nd (III). Journal of Chemical & Engineering Data. 2010;55(12):5759-65.
99. Choi SH, Pang K, Kim K, Churchill DG. Cu2+ Colorimetric Sensing and Fluorescence Enhancement and Hg2+ Fluorescence Diminution in “Scorpionate”-like Tetrathienyl-Substituted Boron− Dipyrrins. Inorganic chemistry. 2007;46(25):10564-77.
100. Xiang Y, Wu F. Study of the interaction between a new Schiff-base complex and bovine serum albumin by fluorescence spectroscopy. Spectrochimica Acta Part A: Molecular and Biomolecular Spectroscopy. 2010;77(2):430-6.
101. Farrokhpour H, Hadadzadeh H, Darabi F, Abyar F, Rudbari HA, Ahmadi-Bagheri T. A rare dihydroxo copper (II) complex with ciprofloxacin; a combined experimental and ONIOM computational study of the interaction of the complex with DNA and BSA. RSC Advances. 2014;4(67):35390-404.
102. Valeur B, Berberan-Santos MN. Molecular fluorescence: principles and applications: John Wiley & Sons; 2012.
103. Samari F, Shamsipur M, Hemmateenejad B, Khayamian T, Gharaghani S. Investigation of the interaction between amodiaquine and human serum albumin by fluorescence spectroscopy and molecular modeling. European journal of medicinal chemistry. 2012;54:255-63.

104. Shahabadi N, Maghsudi M, Rouhani S. Study on the interaction of food colourant quinoline yellow with bovine serum albumin by spectroscopic techniques. Food chemistry. 2012;135(3):1836-41.
105. Kang T-S, Mao Z, Ng C-T, Wang M, Wang W, Wang C, et al. Identification of an iridium (III)-based inhibitor of tumor necrosis factor-α. Journal of medicinal chemistry. 2016;59(8):4026-31.
106. Krishnamoorthy P, Sathyadevi P, Butorac RR, Cowley AH, Bhuvanesh NS, Dharmaraj N. Copper (I) and nickel (II) complexes with 1: 1 vs. 1: 2 coordination of ferrocenyl hydrazone ligands: Do the geometry and composition of complexes affect DNA binding/cleavage, protein binding, antioxidant and cytotoxic activities? Dalton Transactions. 2012;41(15):4423-36.
107. Zhao X, Lu D, Hao F, Liu R. Exploring the diameter and surface dependent conformational changes in carbon nanotube-protein corona and the related cytotoxicity. J Hazard Mater. 2015;292:98-107.
108. Fu X-B, Weng G-T, Liu D-D, Le X-Y. Synthesis, characterization, DNA binding and cleavage, HSA interaction and cytotoxicity of a new copper (II) complex derived from 2-(2′-pyridyl) benzothiazole and glycylglycine. J Photochem Photobiol, A. 2014;276:83-95.
109. Zhao X, Liu R, Chi Z, Teng Y, Qin P. New insights into the behavior of bovine serum albumin adsorbed onto carbon nanotubes: comprehensive spectroscopic studies. J Phys Chem B. 2010;114(16):5625-31.
110. Ao J, Gao L, Yuan T, Jiang G. Interaction mechanisms between organic UV filters and bovine serum albumin as determined by comprehensive spectroscopy exploration and molecular docking. Chemosphere. 2015;119:590-600.
111. Hemmateenejad B, Shamsipur M, Samari F, Khayamian T, Ebrahimi M, Rezaei Z. Combined fluorescence spectroscopy and molecular modeling studies on the interaction between harmalol and human serum albumin. J Pharm Biomed Anal. 2012;67:201-8.
112. Etaiw SEH, El-Aziz DMA, El-Zaher EHA, Ali EA. Synthesis, spectral, antimicrobial and antitumor assessment of Schiff base derived from 2-aminobenzothiazole and its transition metal complexes. Spectrochimica Acta Part A: Molecular and Biomolecular Spectroscopy. 2011;79(5):1331-7.
113. Yang Z-Y, Yang R-D, Li F-S, Yu K-B. Crystal structure and antitumor activity of some rare earth metal complexes with Schiff base. Polyhedron. 2000;19(26):2599-604.
114. Mladenova R, Ignatova M, Manolova N, Petrova T, Rashkov I. Preparation, characterization and biological activity of Schiff base compounds derived from 8-hydroxyquinoline-2-carboxaldehyde and Jeffamines ED®. European polymer journal. 2002;38(5):989-99.
115. Walsh O, Meegan M, Prendergast R, Al Nakib T. Synthesis of 3-acetoxyazetidin-2-ones and 3-hydroxyazetidin-2-ones with antifungal and antibacterial activity. European Journal of Medicinal Chemistry. 1996;31(12):989-1000.

Highlights

- A novel Cu(II) distorted cubane complex containing Cu_4O_4 core, was synthesized and characterized.
- The complex was reported as a tetranuclear catalyst for temperature dependent oxidation of 3,5-di-*tert*-buthyl catechol.
- Interaction of the complex with DNA & protein (BSA) was studied.
- *In vitro* anticancer activity of the complex was evaluated against A549, Jurkat and Ragi cell lines by MTT assay.

Declaration of interest

This article has not been published previously and it is not under consideration for publication elsewhere. This manuscript is approved by all authors and tacitly or explicitly by the responsible authorities where the work was carried out, and that, if accepted, it will not be published elsewhere in the same form, in English or in any other language, including electronically without the written consent of the copyright-holder.